

1

2 The tumor suppressor APC is an attenuator of spindle-  
3 pulling forces during *C. elegans* asymmetric cell division

4

5 **-Author names and Affiliations**

6 Kenji Sugioka<sup>1,2,3</sup>, Lars-Eric Fielmich<sup>4</sup>, Kota Mizumoto<sup>2</sup>, Bruce Bowerman<sup>3</sup>, Sander  
7 van den Heuvel<sup>4</sup>, Akatsuki Kimura<sup>5,6</sup> and Hitoshi Sawa<sup>1,2,6</sup>

8 <sup>1</sup>Multicellular Organization Laboratory, National Institute of Genetics, 1111 Yata,  
9 Mishima, 411-8540 Japan

10 <sup>2</sup>RIKEN Center for Developmental Biology, 2-2-3 Minatojima-minamimachi, Chuo-  
11 ku, Kobe 650-0047 Japan

12 <sup>3</sup>Institute of Molecular Biology, University of Oregon, Eugene, OR 97403 USA

13 <sup>4</sup>Developmental Biology, Biology Department, Utrecht University, Padualaan 8,  
14 3584 CH, Utrecht, Netherlands

15 <sup>5</sup>Cell Architecture Laboratory, National Institute of Genetics, 1111 Yata,  
16 Mishima, 411-8540 Japan

17 <sup>6</sup>Department of Genetics, School of Life Science, Sokendai, 1111 Yata, Mishima,  
18 411-8540 Japan

19

20 **-Corresponding authors**

21 Hitoshi Sawa

22 Multicellular Organization Laboratory, National Institute of Genetics, 1111 Yata,

23 Mishima, 411-8540 Japan

1 hisawa@nig.ac.jp

2 Phone: +81-55-981-6845

3 Fax: +81-55-981-6846

4

5 Akatsuki Kimura

6 Cell Architecture Laboratory, National Institute of Genetics, 1111 Yata,

7 Mishima, 411-8540 Japan

8 akkimura@nig.ac.jp

9

10 Sander van den Heuvel

11 Developmental Biology, Biology Department, Utrecht University, Padualaan 8,

12 3584 CH, Utrecht, Netherlands

13 S.J.L.vandenHeuvel@uu.nl

14

15 Present address:

16 Kota Mizumoto

17 Department of Zoology, the University of British Columbia, Vancouver, Canada,

18 V6T 1Z3

19

20

1 **Abstract**

2 The adenomatous polyposis coli (APC) tumor suppressor has dual functions in  
3 Wnt/ $\beta$ -catenin signaling and accurate chromosome segregation, and is frequently  
4 mutated in colorectal cancers. Although APC contributes to proper cell division, the  
5 underlying mechanisms remain poorly understood. Here we show that *C. elegans*  
6 APR-1/APC is an attenuator of the pulling forces acting on the mitotic spindle.  
7 During asymmetric cell division of the *C. elegans* zygote, a LIN-5/NuMA protein  
8 complex localizes dynein to the cell cortex, to generate pulling forces on astral  
9 microtubules that position the mitotic spindle. We found that APR-1 localizes to the  
10 anterior cell cortex in a Par-aPKC polarity-dependent manner and suppresses anterior  
11 centrosome movements. Our combined cell biological and mathematical analyses  
12 support the conclusion that cortical APR-1 reduces force generation by stabilizing  
13 microtubule plus ends at the cell cortex. Furthermore, APR-1 functions in  
14 coordination with LIN-5 phosphorylation to attenuate spindle pulling forces. Our  
15 results document a physical basis for spindle-pulling force attenuation, which may be  
16 generally used in asymmetric cell division, and when disrupted potentially contributes  
17 to division defects in cancer.

18

19

20

21

22

23

24

1

## 2 **Introduction**

3

4 The mitotic spindle segregates chromosomes and determines the plane of cell  
5 cleavage during animal cell division. Forces that act on the mitotic spindle regulate its  
6 position to produce daughter cells of the proper size, fate and arrangement, thereby  
7 playing a significant role in asymmetric cell division, tissue integrity and  
8 organogenesis. In various organisms, cells regulate spindle positioning through  
9 cortical force generators that pull on astral microtubules (Siller and Doe, 2009;  
10 Knoblich, 2010; Williams and Fuchs, 2013; Rose and Gönczy, 2014; di Pietro et al.,  
11 2016). An evolutionarily conserved force generator complex, consisting of LIN-  
12 5/NuMA, GPR-1,2/LGN and  $G\alpha$ , interacts with dynein and dynamic astral  
13 microtubules to position the mitotic spindle during the asymmetric divisions of the *C.*  
14 *elegans* early embryo (Rose and Gönczy, 2014), *Drosophila* and mammalian  
15 neuroblasts (Siller and Doe, 2009; Knoblich, 2010), and skin stem cells (Williams and  
16 Fuchs, 2013). Although Par-aPKC polarity and cell cycle regulators are known to  
17 control spindle positioning (Rose and Gönczy, 2014; Portegijs et al., 2016), how the  
18 forces are regulated spatiotemporally to position the spindle in various cell types  
19 during development remains poorly understood.

20 The tumor suppressor adenomatous polyposis coli (APC) is a widely  
21 conserved multifunctional protein with two major roles. First, APC functions as part  
22 of a degradation complex to down-regulate  $\beta$ -catenin-TCF dependent transcription,  
23 thereby controlling cell fate and proliferation in various cell types (Clevers and Nusse,  
24 2012). Second, APC functions as a microtubule-associated protein to stabilize MTs,  
25 thereby regulating cell migration (Barth et al., 2008; Etienne-Manneville, 2009),

1 spindle orientation (Pereira and Yamashita, 2011; Yamashita et al., 2003), and  
2 chromosome segregation (Bahmanyar et al., 2009; Rusan and Peifer, 2008). In  
3 mammals, loss of the former function is closely associated with colon cancer (Moser  
4 et al., 1992; Su et al., 1992). Loss of the latter function causes spindle positioning  
5 defects (Beamish et al., 2009; Green et al., 2005) and chromosome instability (CIN)  
6 (Fodde et al., 2001; Green and Kaplan, 2003; Kaplan et al., 2001), a hallmark of  
7 metastatic tumors (Hanahan and Weinberg, 2011), suggesting that the cytoskeletal  
8 roles of APC during mitosis are also relevant for oncogenesis. How APC regulates the  
9 mitotic spindle remains poorly understood and is complicated by its multiple  
10 functions, binding-partners and cellular locations (Bahmanyar et al., 2009; Nelson and  
11 Näthke, 2013).

12         Yeast and fly studies have suggested that APC at the cell cortex contributes to  
13 mitotic spindle positioning. Kar9, an APC-related protein in budding yeast, localizes  
14 asymmetrically to the cell cortex of budding daughter cells through type V myosin-  
15 dependent transport of growing microtubule ends (Hwang et al., 2003; Korinek et al.,  
16 2000; Lee et al., 2000). Cortical Kar9 captures microtubules (MTs) by binding yeast  
17 EB1, and promotes alignment of the spindle along the mother-bud axis (Miller and  
18 Rose, 1998; Korinek et al., 2000; Lee et al., 2000; Siller et al., 2006). *Drosophila*  
19 APC2 predominantly localizes to the cell cortex in syncytial embryos. APC2 mutants  
20 show a CIN phenotype, presumably because APC2 is required for proper centrosome  
21 separation (Poulton et al., 2013). The forces that mediate centrosome separation have  
22 been proposed to depend on APC2 connecting astral MTs to cortical actin (Poulton et  
23 al., 2013). However, the mechanism by which cortical APC regulates spindle-pulling  
24 forces has not been directly addressed in any organism.

1           We report here that loss of cortical APR-1/APC disrupts asymmetries in  
2 spindle movements during mitotic division of the *C. elegans* zygote. In wild-type  
3 embryos, the net pulling forces acting on the mitotic spindle become higher in the  
4 posterior compared to the anterior, causing the spindle to move posteriorly during  
5 metaphase and anaphase (spindle displacement) (Galli and van den Heuvel, 2008;  
6 Gönczy, 2008). In anaphase, the posterior spindle pole swings along the transverse  
7 axis (spindle oscillation), while the anterior pole remains relatively stable. We found  
8 APR-1 to be enriched at the anterior cortex in a PAR-polarity dependent manner.  
9 Loss of APR-1 resulted in anterior pole oscillations that resembled those of the  
10 posterior pole. Laser-mediated spindle severing showed that the spindle-pulling forces  
11 acting on the anterior spindle pole were increased in *apr-1(RNAi)* embryos. Using live  
12 imaging and numerical simulation, we found that the APR-1 dependent stabilization  
13 of MT-cortex interactions negatively regulated the pulling forces acting on the  
14 anterior centrosome in wild-type zygotes. Our study demonstrates that APR-1 is an  
15 attenuator of spindle-pulling forces, and improves our understanding of how cortical  
16 polarity precisely regulates spindle positioning during asymmetric cell division.  
17

## 1 **Results**

### 2 **APR-1/APC localizes asymmetrically to the cell cortex in a PAR and Frizzled** 3 **protein dependent manner**

4 We have previously shown that APR-1 localizes asymmetrically to the anterior cortex  
5 in the EMS blastomere at the six-cell stage and in post-embryonic seam cells, in  
6 response to Wnt signals that regulate the asymmetry of these divisions (Mizumoto and  
7 Sawa, 2007; Sugioka et al., 2011). While analyzing GFP::APR-1 localization in early  
8 embryos, we noticed that APR-1 also is asymmetrically localized in the zygote, called  
9 P0, where roles for Wnt signaling have not been reported. APR-1 formed dot-like  
10 particles that were enriched within the anterior cortex throughout P0 cell division  
11 (APR-1 asymmetry) (Figure 1A). We quantified the number of APR-1 dots by  
12 counting the fluorescent foci with a signal above a threshold (see Materials and  
13 methods). Although the foci numbers changed from prophase to metaphase, and from  
14 anaphase to telophase, we observed anterior enrichment of APR-1 foci throughout the  
15 cell cycle (Figure 1A and 1D).

16 It is well-established that the Par-aPKC system generates anterior-posterior  
17 (A-P) cell polarity to regulate the asymmetric division of P0, through interactions  
18 between anterior (PAR-3, PAR-6, PKC-3) and posterior (PAR-2, PAR-1) *partitioning*  
19 *defective* (PAR) proteins at the cell cortex (Figure 1B; Munro and Bowerman, 2009).  
20 We found that APR-1 asymmetry in P0 was disrupted after RNAi knockdown of *par-*  
21 *3*, *pkc-3* or *par-2* (Figure 1C, 1E, and Figure S1), suggesting that its asymmetry is  
22 established through the Par-aPKC system.

23 In EMS and seam cells, the establishment of APR-1 asymmetry depends on  
24 Wnt proteins (Mizumoto and Sawa, 2007; Sugioka et al., 2011). In P0, MOM-2 is the  
25 only Wnt protein that is maternally provided as mRNA (Harterink et al., 2011),

1 although the mRNA appears not to be translated until the 4-cell stage (Oldenbroek et  
2 al., 2013). As expected, we found that APR-1 localization was not affected in *mom-*  
3 *2(or309)* null mutants, suggesting that the APR-1 asymmetry in P0 does not require  
4 Wnt ligands (Figure 1C, 1E, and Figure S1).

5 Despite the lack of a requirement for MOM-2/Wnt, we observed altered APR-  
6 1 localization after RNAi knockdown of downstream Wnt signaling components.  
7 Specifically, knockdown of the Frizzled receptor MOM-5 or simultaneous inhibition  
8 of the Dishevelled homologs, DSH-2 and MIG-5, increased the numbers of APR-1  
9 foci in both the anterior and posterior cortex without altering APR-1 expression levels  
10 (Figure 1C, 1E, Figure S1, Figure S2A and S2C). Inhibition of WRM-1/ $\beta$ -catenin did  
11 not affect APR-1 localization, and *mom-5(RNAi)* as well as *dsh-2;mig-5(RNAi)*  
12 embryos still showed APR-1 asymmetry (Figure 1C, 1E, Figure S1, S2A and S2B).  
13 DSH-2 localizes to the posterior cell cortex during Wnt-dependent asymmetric cell  
14 divisions later in development (Mizumoto and Sawa, 2007; Walston et al., 2004). In  
15 contrast, DSH-2 localization in P0 was not asymmetric (Figure S2D), consistent with  
16 the lack of Dishevelled requirement in APR-1 asymmetry. We conclude that the Par-  
17 aPKC system establishes APR-1 asymmetry in P0, while Frizzled and Dishevelled  
18 negatively regulate the levels of cortical APR-1.

19

## 20 **APR-1 asymmetrically suppresses centrosome movements during P0 cell division**

21 The Par-aPKC system independently regulates two P0 asymmetries: the segregation  
22 of cell fate determinants (e.g. PIE-1 and PGL-1) and posterior mitotic spindle  
23 displacement. In *apr-1(RNAi)* embryos, GFP::*PIE-1* and GFP::*PGL-1* segregated into  
24 the posterior daughter cell as in wild-type embryos, indicating that APR-1 is not  
25 involved in cytoplasmic determinant localization (Figure S2E and data not shown). In

1 contrast, *apr-1(RNAi)* embryos showed abnormal spindle oscillations. In the wild type,  
2 posterior spindle displacement starts during metaphase and continues during anaphase  
3 when it coincides with transverse oscillations of the two spindle poles (Figure 2A and  
4 2B). The posterior spindle pole oscillates more vigorously than the anterior pole  
5 (Figure 2C and Video 1), as a result of higher posterior than anterior cortical pulling  
6 forces (Pecreaux et al., 2006). In *apr-1(RNAi)* embryos, the mitotic spindle moved  
7 back and forth along the A-P axis (Figure 2B, 2D, and Video 2), and the anterior  
8 spindle pole exhibited excessive transverse oscillations (Figure 2C, 2E, 2F, and Video  
9 2). These data indicate that APR-1 suppresses anterior spindle pole movements and  
10 hence overall spindle positioning during posterior displacement.

11 In *mom-5(ne12)* null mutant embryos, in which APR-1 was also enriched at  
12 the posterior cell cortex, we observed reduced posterior spindle pole oscillations  
13 (Figure S3A and S3B). However, spindle pole oscillations were not restored in *apr-*  
14 *1(RNAi); mom-5(null)* embryos (Figure S3B). We noticed that *mom-5(null)* and *apr-*  
15 *1(RNAi); mom-5(null)* embryos were smaller in size, potentially limiting spindle pole  
16 oscillations through spatial effects (Figure S3C). Therefore, we could not determine  
17 the effects of excess cortical APR-1 on spindle pole movements in the *mom-5(null)*  
18 background. However, in other aspects of spindle dynamics described below, elevated  
19 cortical localization potentiated APR-1 function.

20

## 21 **APR-1 asymmetrically stabilizes microtubule-cortex interactions**

22 As mammalian APC (Zumbrunn et al., 2001) and *C. elegans* APR-1 in the EMS cell  
23 (Sugioka et al., 2011) can stabilize MTs, we hypothesized that anteriorly enriched  
24 APR-1 in the P0 cell may also increase MT stability at the cell cortex to regulate  
25 asymmetric spindle movements. To assess this possibility, we analyzed the MT-

1 cortex interactions using live imaging of GFP:: $\beta$ -tubulin expressing embryos. In  
2 kymographs of midplane images, astral microtubules appear to persist longer on the  
3 anterior cell cortex than on the posterior, consistent with previous observations  
4 (Figure 3A; Labbé et al., 2003). To quantify MT-plus end residence time at the cortex,  
5 we measured the duration of GFP:: $\beta$ -tubulin foci on the flattened cell surface (Figure  
6 3B). Most of the GFP:: $\beta$ -tubulin foci initially co-localized with the EB1-related plus-  
7 end binding protein EBP-2 (96.1%; n = 255), confirming that the foci represent MT  
8 plus-ends. Shortly after the cortical attachment, EB1 dissociates from MT plus-ends,  
9 while some MTs remained at the cortex after the release of EB1 (Fig. 3B and 3D).  
10 The numbers of such long-lived microtubule plus-ends were higher anteriorly,  
11 accounting for the asymmetry in cortical MT residence time in wild-type zygotes  
12 (Figure 3B-3D; red arrows in 3C, Video 3 and Video 4).

13 Notably, the MT residence time at the anterior cortex was significantly lower  
14 in *apr-1(RNAi)* embryos than in the wild type (Figure 3C, 3E and Video 5). In  
15 contrast, *mom-5* mutants with excess cortical APR-1 showed an increased MT  
16 residence time at both the anterior and posterior cell cortex (Figure 3C, 3E and Video  
17 6). RNAi knockdown of *apr-1* overcame this *mom-5* phenotype, reducing MT cortical  
18 residence throughout the cortex (Figure 3C, 3E and Video 7). Thus, APR-1 stabilizes  
19 microtubule-cortex interactions and acts downstream of MOM-5 (Figure 4D).

20

### 21 **APR-1 asymmetrically attenuates pulling forces acting on the mitotic spindle**

22 The exaggerated anterior spindle pole movements in *apr-1(RNAi)* embryos implicate  
23 APR-1 in spindle-pulling force regulation. We investigated this possibility using  
24 spindle severing assays (Figure 4A; Grill et al., 2001). After cutting the spindle  
25 midzone with a UV laser, the average peak velocities of the anterior and posterior

1 spindle poles moving toward the cell cortex were calculated (Figure 4A). In control  
2 embryos, the posterior spindle pole moved faster than the anterior pole, as expected  
3 (Figure 4A, 4B, and Video 8). In *apr-1(RNAi)* embryos, we observed an increased  
4 average peak velocity specifically for the anterior spindle pole (Figure 4A, 4B, and  
5 Video 8). In *mom-5(null)* embryos with excess cortical APR-1, both the anterior and  
6 posterior spindle poles showed reduced average peak velocities (Figure 4B and Video  
7 8). Combined *apr-1(RNAi);mom-5(null)* embryos showed increased average peak  
8 velocities and resembled *apr-1(RNAi)* embryos (Figure 4B and Video 8). These  
9 results indicate that the cortical levels of APR-1 inversely correlate with spindle-  
10 pulling forces (Figure 4D).

11

### 12 **APR-1-dependent stabilization of MTs accounts for reduced pulling forces on** 13 **the anterior spindle pole**

14 We have shown that APR-1 is enriched in the anterior cell cortex, promotes cortical  
15 MT residence times anteriorly, and suppresses both spindle-pulling forces and  
16 anterior spindle pole oscillations, raising the possibility that all of these processes are  
17 mechanistically linked. It has been shown that cortical pulling forces are generated  
18 when MTs reaching the cortex meet dynein and undergo catastrophe (Laan et al.,  
19 2012). Therefore, we hypothesized that cortical APR-1 reduces the MT catastrophe  
20 frequency and thereby attenuates force generation and spindle movement. However, it  
21 is not clear whether the magnitude of APR-1-dependent cortical MT stabilization is  
22 sufficient to suppress spindle movement.

23 We decided to examine this issue using numerical simulation. First, we  
24 estimated MT catastrophe frequencies from their cortical residence time  
25 (Supplementary Table 1, Figure S4). In control embryos, the estimated catastrophe

1 frequency at the anterior cortex was about half of that at the posterior cortex. Such a  
2 reduced catastrophe frequency was not detected at the anterior cortex of *apr-1(RNAi)*  
3 embryos, indicating that in wild type embryos the catastrophe frequency is suppressed  
4 by APR-1.

5 We set the rescue frequency of all MTs high, so that soon after the MTs start  
6 to shorten, they regrow to reach the cortex (Supplemental Table 2). This assumption  
7 was introduced to make the number of MTs reaching the cortex almost constant  
8 regardless of the differences in catastrophe frequencies between anterior and posterior,  
9 which is the case in living embryos (Video 3). Without this assumption, the number  
10 of MTs reaching the cortex should be ~2-fold higher at the anterior because the  
11 catastrophe frequency is about half. The mechanistic bases of this assumption is  
12 provided by the *in vivo* observation that individual microtubules appear to form  
13 bundles, and multiple EB1 tracks move along a bundled fiber toward the cell cortex,  
14 making rescue frequency of the fiber higher than individual MTs (Video 4).

15 We conducted 3-dimensional simulations of spindle movements. As in  
16 previous simulations (Hara and Kimura, 2009; Kimura and Onami, 2005, 2007;  
17 Kimura and Onami, 2010), the spindle moves as a result of three kinds of forces  
18 acting on astral MTs that radiate from each spindle pole (Figure 2G). First, all MTs  
19 generate pulling forces proportional to their length (“cytoplasmic pulling force”). This  
20 force is important for bringing the spindle to the cell center (Hamaguchi and Hiramoto,  
21 1986; Kimura and Onami, 2005; Kimura and Kimura, 2011), and is also critical for  
22 oscillation (Pecreaux et al., 2006). Second, MTs that reach the cell cortex generate the  
23 pulling force at their plus ends only when they undergo catastrophe (“cortical pulling  
24 force”). The current theory for the basis of oscillation is that when the spindle poles  
25 move toward one side, the pulling force from that side becomes stronger (“positive

1 feedback” or “negative friction”), while the opposing centering force also increases  
2 (Grill et al., 2005; Pecreaux et al., 2006; Vogel et al., 2009). With this mechanism, the  
3 spindle is not stabilized at the center but oscillates. In our model, the frequency of the  
4 force generation depends on the number of active cortical force generators and the  
5 MT residence time controlled by APR-1, both of which have A-P asymmetry. The  
6 third force connects the anterior and posterior spindle poles. We assumed a spring-  
7 like connection between the poles that was weakened after anaphase onset to mimic  
8 the spindle elongation.

9 Numerical simulations were conducted for control, *apr-1(RNAi)* and *mom-*  
10 *5(null)* situations (Figure S5), by setting the catastrophe frequency to values estimated  
11 from experimental data (e.g. 0.31 /s for the anterior and 0.72 /s for the posterior, see  
12 Supplementary Table 1). The simulation results indicated that the APR-1-dependent  
13 stabilization of MTs is sufficient to suppress oscillation of the anterior pole (Figure  
14 2H). In wild-type simulations, the spindle moved toward the posterior and elongated  
15 upon anaphase onset (Figure S5A and Video 9). The oscillations perpendicular to the  
16 A-P axis were also reproduced for both spindle poles (Figure S5B). In *apr-1(RNAi)*  
17 simulations, in which the catastrophe frequency at the anterior cortex was increased,  
18 the amplitude of the anterior spindle pole oscillations was increased (Figure 2H and  
19 Video 9). Furthermore, the average peak velocities of anterior poles in the severing  
20 experiments were also consistent with the forces acting on anterior spindle poles in  
21 our simulations (Figure 4C). Overall, the numerical simulations demonstrated that the  
22 APR-1-dependent stabilization of MTs at the cortex can suppress spindle pole  
23 oscillations through the reduction of force generation.

24

1 **Anterior APR-1 and LIN-5 phosphorylation together attenuate spindle pulling**  
2 **forces**

3 We investigated the significance of spindle pulling force attenuators in asymmetric  
4 cell division. Along with APR-1, we focused on the LIN-5 protein. LIN-5 presumably  
5 interacts with cortical GPR-1/2 and dynein in cortical force generation (Nguyen-Ngoc  
6 et al., 2007). We have previously reported that anteriorly-localized PKC-3/aPKC  
7 phosphorylates LIN-5 to attenuate cortical-pulling forces (Galli et al., 2011). We  
8 edited the *lin-5* genomic locus to substitute four aPKC phosphorylated serine residues  
9 with alanine by CRISPR/Cas9-mediated homologous recombination. In the obtained  
10 mutant (*lin-5 4A*), the average peak velocities of the anterior and posterior poles were  
11 still asymmetric, although they were increased compared to the control (Figure 5A).  
12 However, when we performed spindle severing in *apr-1(RNAi); lin-5 4A* embryos, the  
13 anterior average peak velocities were further enhanced and no longer significantly  
14 different from those of the posterior pole (Figure 5A). These data suggest that the Par-  
15 aPKC-dependent asymmetric localization of APR-1 and phosphorylation of LIN-5  
16 together attenuate cortical pulling forces, as a major cause of the pulling force  
17 asymmetry that positions the mitotic spindle (Figure 5B-5D).

18

## 1 **Discussion**

2 In this study, we investigated how the APR-1/APC protein regulates mitotic spindle  
3 movements in the *C. elegans* one-cell embryo, a well-established model for  
4 asymmetric cell division. We observed that APR-1/APC becomes asymmetrically  
5 enriched at the anterior cell cortex, dependent on the Par-PKC-3 polarity pathway.  
6 We found APR-1 attenuates spindle pulling forces, most likely through stabilization of  
7 MTs at the anterior cell cortex. In concert, Wnt signaling mediated by MOM-  
8 5/Frizzled and Disheveled proteins suppressed cortical accumulation of APR-1,  
9 thereby also contributing to the correct levels of pulling forces. To test these  
10 assumptions, we performed numerical simulations, which closely mimicked the  
11 spindle movements in wild-type and mutant embryos. These combined data strongly  
12 support the conclusion that MT stabilization by APR-1 contributes to correct spindle  
13 positioning. Finally, we provide evidence that APR-1 enrichment and PKC-3  
14 phosphorylation of LIN-5 act in parallel to reduce anterior-directed pulling forces.  
15 These conclusions are likely to apply broadly and improve our understanding of the  
16 microtubule-associated functions of APC.

17 Although APC is a component of Wnt signaling, it has been reported that its  
18 localization is regulated by the Par-aPKC polarity pathway in migrating mammalian  
19 astrocytes (Etienne-Manneville and Hall 2003), and during axonal differentiation of  
20 developing hippocampal neurons (Shi et al., 2004), as we observed in the *C. elegans*  
21 one-cell embryo. Scratching of astrocyte monolayers in wound-healing assays triggers  
22 APC localization to the cell cortex at the leading edge, in response to CDC42-induced  
23 Par-aPKC polarity and Wnt5a signaling (Schlessinger et al., 2007). Interestingly,  
24 polarity establishment in this system is followed by centrosome re-orientation through  
25 APC-microtubule interactions (Etienne-Manneville and Hall 2003). Thus, the

1 mechanisms that control centrosome positioning through interactions between Par  
2 polarity, Wnt signaling, and the APC may be conserved across species.

3         While the roles of cortical APC have been unclear, it was previously proposed  
4 that it stabilizes microtubules through microtubule plus-end binding protein EB1  
5 (Etienne-Manneville and Hall, 2003; Gundersen et al., 2004). Consistently, in the *C.*  
6 *elegans* EMS blastomere, cortical APC stabilizes MT ends coated with EB1 (Sugioka  
7 et al., 2011). However, a few examples including the present study indicate that  
8 cortical APC can stabilize microtubules independently of EB1. First, truncated  
9 mammalian APC that lacks the EB1 interaction domain has been shown to localize to  
10 the cell cortex and to MTs in epithelial cells (Reilein and Nelson, 2005). In addition,  
11 *Drosophila* APC2, which lacks the C-terminal EB1 binding domain, interacts with  
12 microtubule plus ends at the cortex and contributes to centrosome segregation  
13 (Poulton et al., 2013). In our study, APR-1 at the anterior cortex stabilizes MTs but  
14 the mean cortical residence time of EBP-2/EB1 was symmetric. We also observed  
15 that the cortical residence time of EB1 is much shorter than that of MTs in P0, as  
16 reported previously (Kozlowski et al., 2007). Therefore, APR-1 at the anterior cortex  
17 of the P0 cell likely stabilizes MTs independently of EB1 binding. We observed  
18 recently that deleting all EB family members has limited effects on spindle behavior  
19 and viability in *C. elegans* (Schmidt et al., 2017). Therefore, the microtubule  
20 stabilizing effects of cortical APC probably do not depend on EB1 protein interaction.

21         Mitotic spindle positioning is controlled during embryogenesis, in various  
22 adult stem cell divisions, and in symmetric divisions (Siller and Doe, 2009; Williams  
23 and Fuchs, 2013; Kiyomitsu and Cheeseman, 2012). While many studies have  
24 focused on the localization of cortical force generators that pull spindles toward them,  
25 attenuators of spindle pulling forces may be just as important in creating asymmetry.

1 In fact, a variety of molecular mechanisms appear to suppress spindle pulling forces  
2 in the one-cell embryo, including PKC-3-mediated LIN-5 phosphorylation (Galli et  
3 al., 2011), cortical actin (Berends et al., 2013), and posterior-lateral LET-99  
4 localization (Krueger et al., 2010). In this study, we provide evidences toward the  
5 understanding of a physical basis of spindle pulling force attenuation: we found that  
6 APC acts as an attenuator of spindle pulling forces, through stabilization of  
7 microtubule plus ends at the cortex. Importantly, a similar force attenuator function of  
8 APC is potentially used in oriented divisions of *Drosophila* germline stem cells  
9 (Yamashita et al., 2003) and mouse embryonic stem cells (ES cells) attached to Wnt-  
10 immobilized beads (Habib et al., 2013), as they exhibit asymmetric APC localizations  
11 similar to what we have observed in the *C. elegans* zygote. Our study also implies that  
12 not only APC but also other proteins involved in MT stabilization are potential  
13 cortical spindle pulling force attenuators.

14 The observed pulling force attenuation function may be relevant for the  
15 chromosomal instability (CIN) phenotype associated with APC loss in human colon  
16 cancer (Fodde et al., 2001; Kaplan et al., 2001). Initial studies of cultured mammalian  
17 cells associated APC loss and CIN with defective kinetochore-microtubule  
18 attachments, although abnormal spindle structures were also observed in APC  
19 defective cells (Fodde et al., 2001; Kaplan et al., 2001). In *Drosophila* embryos,  
20 APC2 was found to localize predominantly to the cell cortex (McCartney et al., 2001).  
21 Chromosome missegregation associated with APC2 loss in such embryos was linked  
22 to a cytoskeletal function of APC in centrosome segregation (Poulton et al., 2013). In  
23 our study, we found that *C. elegans* APC localizes to the cell cortex where it  
24 negatively regulates spindle-pulling forces. Consequently, the absence of APC results  
25 in increased pulling forces exerted on the spindle poles. Interestingly, defective

1 kinetochore attachments have been shown to cause chromosome segregation defects  
2 in *C. elegans*, in a manner dependent on cortical pulling forces (Cheeseman et al.,  
3 2005). Thus, combining these data with our results raises a new and testable  
4 hypothesis that increased cortical-pulling forces and abnormal MT-kinetochore  
5 interactions synergistically elevate the risk of CIN in developing tumors with APC  
6 mutations.

7

8

9

10

## 1 **Materials and methods**

### 2 ***C. elegans* culture and strains**

3 All strains used in this study were cultured by standard methods (Brenner, 1974).  
4 Most worms were grown at 20 °C or 22.5 °C and then incubated at 25 °C for  
5 overnight before the analysis. Worm used for anti-DSH-2 staining were grown at 22.5  
6 °C. Worms carrying PIE-1::GFP were grown at 15°C and incubated at 25°C for  
7 overnight before the analysis. The following allele were used: *mom-2(or309)*, *mom-*  
8 *5(ne12)*, *par-2(it51)*. We used *mom-5(ne12)* null mutants for all experiments except  
9 those in Figure 1. The following integrated transgenic lines were used: *osIs15*  
10 (Sugioka et al., 2011) for GFP::APR-1; *ruls32* (Praitis et al., 2001) for GFP::H2B;  
11 *ojIs1* (Strome et al., 2001) for GFP::β-tubulin; *axIs1462* (Merritt et al., 2008) for  
12 GFP::PIE-1; *axIs1720* (Merritt et al., 2008) for GFP::PGL-1; *tjIs8* for GFP::EBP-1;  
13 *ruls57* for GFP::tubulin. We also generated EBP-2::mKate2 fusion strain *ebp-*  
14 *2(or1954[ebp-2::mKate2])* and *lin-5* 4A strain by CRISPR/Cas9 genome editing as  
15 described below.

16

### 17 **Generation of CRISPR repair templates**

18 For the generation of *ebp-2::mKate2* strain, CRISPR repair constructs containing 700  
19 bp homologous arms were synthesized as gBlock fragments (Integrated DNA  
20 Technologies, Coralville, IA) and assembled into pJET2.1 vector using in-house  
21 Gibson Assembly reaction mix (Gibson et al., 2009). For the generation of *lin-5* 4A  
22 strain, CRISPR repair constructs were inserted into the pBSK vector using Gibson  
23 Assembly (New England Biolabs, Ipswich, MA). Homologous arms of at least 1500  
24 bp upstream and downstream of the CRISPR/Cas9 cleavage site were amplified from  
25 cosmid C03G3 using KOD Polymerase (Novagen (Merck) Darmstadt, Germany).

1 Linkers containing the point mutations were synthesized (Integrated DNA  
2 technologies, Coraville, IA). Mismatches were introduced in the sgRNA target site to  
3 prevent cleavage of knockin alleles. All plasmids and primers used for this study are  
4 available upon request.

5

## 6 **CRISPR/ Cas9 genome editing**

7 Young adults were injected with solutions containing the following injection mix. For  
8 *ebp-2::mKate2*, 10 ng/μl pDD162 *Peft-3::Cas9* with sgRNA targeting C-terminus of  
9 *ebp-2* locus (Addgene 47549; Dickinson et al., 2013), 10 ng/μl repair template, and  
10 65 ng/μl selection marker pRF4 were used. For *lin-5* 4A, 50 ng/μl *Peft-3::Cas9*  
11 (Addgene 46168; Friedland et al., 2013), 50 ng/μl of two PU6::sgRNAs targeting the  
12 region of the four serine residues to be mutated to alanine, 50 ng/μl repair template  
13 and 2.5 ng/μl selection marker *Pmyo-2::tdTomato* were used. Progeny of animals that  
14 carry selection markers were transferred to new plates 3–4 days post injection. For  
15 *ebp-2::mKate2*, GFP positive animals were crossed with a strain carrying GFP::  
16 tubulin to obtain *ebp-2::mKate2* with GFP::tubulin (EU3068; *ebp-2(or1954[ebp-*  
17 *2::mKate2]* II). For *lin-5* 4A, PCRs with primers diagnostic for recombination  
18 products at the endogenous locus were performed on F2-F3 populations, where one  
19 primer targeted the altered base pairs in the sgRNA site and point mutations and the  
20 other just outside the homology arm. The resulting strain (SV1689; *lin-5*  
21 (*he260[S729A/S734A/S737A/S739A]* II) was crossed with AZ244 (*unc-119(ed3)*  
22 III; *ruIs57*) to obtain the *lin-5* 4A strain with GFP::tubulin (SV1690; *lin-5(he260);*  
23 *ruIs57*).

24

## 25 **RNAi**

1 DNA fragments corresponding to nucleotide 848-1547 of the *apr-1* cDNA were  
2 amplified and used for the production of the dsRNA and feeding RNAi. For the  
3 experiments in Figure 5, we injected the dsRNA into the gonad and worms were  
4 subsequently cultured under feeding RNAi at 25 °C for over 16 hrs before dissecting  
5 embryos. For the rest of experiments, after injection of the dsRNA into the gonad,  
6 worms were incubated at 25 °C without feeding RNAi for over 30 hrs before  
7 dissecting embryos.

8

### 9 **Microscopy and analysis of living embryos**

10 All embryos were dissected in an egg salt buffer from gravid hermaphrodites (Edgar,  
11 1995). For live imaging except for the experiments in Figure 5, the embryos were  
12 mounted on 4 % agar pads under a coverslip and sealed with petroleum jelly. For  
13 most of the experiments embryos were observed at room temperature by a CSU10  
14 spinning-disc confocal system (Yokogawa Electric, Musashino, Japan) mounted on an  
15 AxioPlan 2 microscope (Carl Zeiss, Oberkochen, Germany) with a Plan-Apochromat  
16 100X 1.4 NA oil immersion lens. The specimens were illuminated with a diode-  
17 pumped solid-state 488 nm laser (HPU50100, 20mW; Furukawa Electric, Tokyo,  
18 Japan). Images were acquired with an Orca ER12-bit cooled CCD camera  
19 (Hamamatsu Photonics, Hamamatsu, Japan), and the acquisition system was  
20 controlled by IP lab software (2 X 2 binning; Milwaukee, WI). Acquired images were  
21 processed with the Image J (Schneider et al., 2012) (NIH) and Adobe Photoshop  
22 (Adobe Systems, San Jose, CA). For the experiments in Figure 3B, images were  
23 captured with a confocal unit CSU-W with Borealis (Andor Technology, Belfast,  
24 Northern Ireland) and dual EMCCD cameras iXon Ultra 897 (Andor Technology)  
25 mounted on an inverted microscope Leica DMI8 (Leica Microsystems, Wetzlar,

1 Germany) controlled by Metamorph (Molecular Devices, Sunnyvale, CA). Spindle  
2 severing experiments were performed with a Micropoint system (Photonic  
3 instruments, St Charles, IL) equipped with a 2 mW pulsed nitrogen laser (model VL-  
4 337; Laser Science Inc., Franklin, MA) exciting Coumarin 440 dye. For the  
5 experiments in Figure 5, embryos were mounted on 4 % agarose pad dissolved in egg  
6 salts buffer and observed by a Nikon Eclipse Ti microscope with Perfect Focus  
7 System (Nikon, Tokyo, Japan) equipped with CSU-X1-A1 spinning disk confocal  
8 head (Yokogawa Electric) and S Fluor 100X 1.3 NA objectives. The specimens were  
9 illuminated with Cobolt Calypso 491 nm laser (Cobolt, Solna, Sweden). Spindle  
10 severing experiments were performed with 355 nm Q-switched pulsed lasers (Teem  
11 Photonics, Meylan, France) with ILas system (Roper Scientific France, Lisses,  
12 France/ PICT-IBiSA, Institut Curie). Temperature was maintained at 25°C by  
13 INUBG2E-ZILCS Stage Top Incubator (Tokai Hit, Fujinomiya, Japan) on the  
14 motorized stage MS-2000-XYZ with Piezo Top plate (ASI, Eugene, OR). Images  
15 were acquired with an Evolve 512 EMCCD camera (Photometrics, Tucson, AZ), and  
16 the acquisition system was controlled by MetaMorph (Molecular Devices).

17

## 18 **Immunostaining**

19 Embryos were fixed and stained with rabbit anti-DSH-2 antibody as described  
20 (Hawkins et al., 2005).

21

## 22 **Measurement of embryo volumes**

23 The volumes (V) of embryos were estimated from the measured embryo length (X)  
24 and width (Y). When three semi-axes of ellipsoid (embryo) in the x, y and z axes are  
25 defined as a, b and c, volume of ellipsoid  $V = 4/3\pi abc$ . With the assumption of equal

1 embryo width in the y and z axes, we estimated a, b and c as 0.5X, 0.5Y and 0.5Y and  
2 calculated V.

3

#### 4 **Statistical analysis**

5 For multiple comparisons, one-way ANOVA with Holm-Sidak's method and Kruskal-  
6 Wallis test followed by Dunn's multiple comparison test were performed for the data  
7 with normal distribution and skewed distribution, respectively. No statistical method  
8 was used to predetermine sample size. The experiments were not randomized. The  
9 investigators were not blinded.

10

#### 11 **Quantification of the data from fluorescence images**

12 For the quantification of the number of dots formed by GFP::APR-1, 8 bit images  
13 were processed with Gaussian blur and segmented with the threshold that covers all  
14 the visible dots using Fiji. Then number of segments were counted by the Image J  
15 plug-in Analyze Particles. For the quantification of total APR-1 level in Figure S2C, 4  
16 successive focal planes including cell center and cell surfaces (corresponding to the  
17 upper half of the cell) were combined by the sum projection and average signal  
18 intensity of cell region was subtracted by that in the area devoid of embryos. For the  
19 quantification of spindle movement, the coordinates of the center of the centrosomes  
20 were analyzed with the Image J plug-in Manual Tracking. For the quantification of  
21 cortical residence times of GFP::EB1 and GFP:: $\beta$ -tubulin, the number of frames from  
22 appearance to disappearance of each dot were counted manually. Note that some MT  
23 dots whose start and end of cortical localization were unclear were not counted. The  
24 average peak velocity after spindle severing was calculated from the distance traveled  
25 by the centrosome center.

1

## 2 **3-dimensional simulation of spindle movement**

3 **Overview.** The simulations included 2 spindle poles connected by a spring with  
4 dynamic astral MTs inside a cell. The cell was simulated as an oval with a long axis  
5 of 50  $\mu\text{m}$  and two short axes of 30  $\mu\text{m}$ . Initial position of the spindle poles is the  
6 center of the cell aligned along the long axis with the distance of 10 $\mu\text{m}$ , which  
7 corresponds to the size of the spindle. The MTs grow and shrink from the spindle  
8 poles stochastically according to the dynamic instability. Depending on the length and  
9 configuration of the MTs, 3 kinds of forces act on spindle poles to move them as  
10 explained below. From an initial configuration, the configuration of the MTs and the  
11 spindle poles was calculated at successive time steps as conducted in previous  
12 simulations (Hara and Kimura, 2009; Kimura and Onami, 2005, 2007; Kimura and  
13 Onami, 2010). The parameters used are listed in Table S2.

14 **Force 1, cytoplasmic pulling forces.** All MTs generate pulling force proportional to  
15 their length. This force is important to bring the spindle at the cell center (Hamaguchi  
16 and Hiramoto, 1986; Kimura and Onami, 2005; Kimura and Kimura, 2011), and is  
17 also critical for oscillation (Pecreaux et al., 2006). The cytoplasmic pulling force  
18 generated for an  $i$ -th MT was modeled as  $F_{\text{cytoplasm}}(i) = D \times L(i) \times F_{FG}(i)$ , where  $D$  is  
19 the density of active force generators in the cytoplasm and  $L(i)$  is the length of the MT.  
20  $F_{FG}(i)$  is same as in the cortical pulling force. The direction of the force is same as the  
21 direction of the MT. We note that the centering force required for oscillation can also  
22 be provided by a force that microtubules produce when they push the cortex (Garzon-  
23 Coral et al., 2016) instead of the cytoplasmic pulling force. The detailed mechanisms  
24 (i.e. pulling or pushing) of the centering force do not affect the overall behavior of our  
25 model.

1 **Force 2, cortical pulling forces.** MTs that reached the cell cortex generate pulling  
2 forces toward their direction only when they start to shrink. The cortical pulling force  
3 generated for an  $i$ -th MT was modeled as  $F_{cortex}(i) = N_{potential}(i) \times P_{active}(i) \times F_{FG}(i)$ .  
4  $N_{potential}$  is the number of force generators that can potentially interact with the MT.  
5 We set this value 30 for posterior cortex and 15 for the anterior cortex. The  
6 experimental value of this parameter has not been investigated, but this number is  
7 consistent with a previous study estimating that the total number of force generators is  
8 less than 50 and the density is double at the posterior cortex compared to anterior one  
9 (Grill et al., 2003).  $P_{active}$  is the probability that the potentially interacting force  
10 generators are active. A critical assumption to generate robust oscillation here is to  
11 model this value high when the spindle pole is approaching the site of the force  
12 generator, and low when the spindle pole is leaving (Grill et al., 2005; Pecreaux et al.,  
13 2006). In the previous study (Pecreaux et al., 2006),  $P_{active}$  was defined as  $P_{active} =$   
14  $p_{mean} + (f'/f_c) \times p_{mean} \times (1 - p_{mean}) \times v - \tau \times (f'/f_c) \times p_{mean} \times (1 - p_{mean}) \times a$ . For simplicity, we  
15 neglected the acceleration term ( $a$ ) and fixed the  $p_{mean}$  parameter to 0.5 to see the  
16 extensive oscillation (Pecreaux et al., 2006). We set  $f'/f_c = 4.0/V_{max}$ , and thus used  
17  $P_{active} = 0.5 + v/V_{max}$ . Here  $v$  is the velocity of the spindle pole toward the direction of  
18 the force generator on the cortex. When  $v < 0$ , we set  $P_{active} = 0$ .  $F_{FG}$  is formulated as  
19  $F_{FG} = F_{stall} (1 - v/V_{max})$  (Kimura and Onami, 2005; Pecreaux et al., 2006). When  $v > V_{max}$ ,  
20 we set  $F_{FG} = 0$ . In the simulation, force generation for shrinking MTs lasts for 100  
21 steps (1 s).  
22 **Force 3, forces connecting the two poles.** To connect the anterior and posterior  
23 spindle poles, which is done by spindle MTs *in vivo*, we treated the spindle as a  
24 Hookean spring. The natural length increases proportionally from 10  $\mu\text{m}$  at time zero  
25 to 12  $\mu\text{m}$  at  $t = 100$  s, which is the onset of anaphase in the simulation. After the onset

1 of anaphase, the natural length increases proportionally to  $22 \mu\text{m}$  at  $t = 200 \text{ s}$ . The  
2 spring constant is high ( $1 \text{ pN}/\mu\text{m}$ ) so that the length of spindle is almost maintained to  
3 the natural length.

4

5

## 6 **Acknowledgements**

7 We thank Nancy Hawkins for the anti-DSH-2 antibody, the *Caenorhabditis* Genetics  
8 Center (funded by the NIH Office of Research Infrastructure Programs; P40  
9 OD010440) for strains. This work was supported by the Netherlands Organization for  
10 Scientific Research (NWO) research program 821.02.001 to SvdH, NIH grant  
11 R01GM049869 to B.B., by the Human Frontier Science Program and NIG  
12 Collaborative Research Program (2013-A60) to K.S., by the Uehara Memorial  
13 Foundation to H.S., and Grants-in-Aid for Scientific Research from the Ministry of  
14 Education, Culture, Sports, Science, and Technology of Japan to H.S (JP22127005)  
15 and A.K. (JP15H04732 and JP15KT0083).

16

## 1 **Figure legends**

### 2 **Figure 1. The Par-aPKC system and Frizzled signaling regulate APR-1**

#### 3 **asymmetric localization during zygote division**

4 (A) GFP::APR-1 signals on the cell surface in different cell cycle stages. In the right  
5 panels, computationally detected APR-1 dots were shown (see Material and Methods).  
6 (B) APR-1 and PAR-6 localizations in the cell midplane during asymmetric cell  
7 division. Schematic drawing shows polarized protein localizations. (C) GFP::APR-1  
8 signals on the cell surface in *mom-2(null)* mutants and *mom-5*, *par-2* or *par-3* RNAi  
9 embryos. (D) Quantified numbers of GFP::APR-1 dots on the anterior and posterior  
10 cell cortex of wild-type embryos in different cell cycle stages. n = 5, 10, 5 from left to  
11 right. (E) Quantified numbers of GFP::APR-1 dots at metaphase or anaphase in RNAi  
12 embryos. n = 10, 7, 10, 9, 10, 10, from left to right. Ends of whiskers indicate  
13 minimum or maximum values. Double asterisk, asterisk and n.s. indicates:  $p < 0.01$ ,  $p$   
14  $< 0.05$  and  $p > 0.05$  (One-way ANOVA with Holm-Sidak's multiple comparison test).  
15 Scale bars are 10 $\mu$ m.

16

### 17 **Figure 2. APR-1 asymmetrically suppresses centrosome movements during the**

#### 18 **P0 cell division**

19 (A) Schematic drawings of spindle movements along the A-P and transverse axes in  
20 fluorescent cells used to generate kymograph in B and C. (B) Kymograph of the  
21 spindle movement along the A-P axis. Weak signals outlined by dotted lines and  
22 strong signals in the center indicate the centrosomes and chromosomes, respectively.  
23 (C) Kymograph of the spindle movement along the transverse axis. (D, E) Trajectory  
24 of centrosome movements. Cell centers are zero in position. (F, H) Total distances for  
25 movements of the anterior and posterior poles in living embryo (F) and in 3D

1 simulations (H). (G) Physical model used for 3D simulation. A and P indicate the  
2 anterior and posterior spindle poles harboring shrinking MTs (orange) and elongating  
3 MTs (blue). Red and black arrows indicate centrosome movements and cortical force  
4 generation. For each MT catastrophe at the cortex, the average pulling forces acting  
5 on single MT at the posterior are stronger than those at the anterior, due to the  
6 different probabilities of MT-force generator interactions (see Materials and methods).  
7 Times are  $\pm 40$  sec and  $\pm 100$  sec relative to the anaphase onset in living embryos and  
8 3D simulations, respectively. Error bars show 95% CI. Double asterisk and n.s.  
9 indicates:  $p < 0.01$  and  $p > 0.05$  compared to control (Kruskal-Wallis test followed by  
10 Dunn's multiple comparison test).

11

12 **Figure 3. APR-1 asymmetrically stabilizes microtubule-cortex interactions.**

13 (A) Kymographs of anterior and posterior cortical microtubules. Using the dotted  
14 lines #1 and #2, anterior and posterior kymographs were generated. (B) Measurement  
15 of cortical MT residence. The embryos were mounted on agarose pads and flattened  
16 by coverslips to visualize cortical microtubule ends in a single focal plane. Examples  
17 of short and long-lived foci were shown below with simultaneous imaging of GFP:: $\beta$ -  
18 tubulin and EB1::mKate2. (C) Cortical microtubule dots in the indicated genotypes  
19 during metaphase-anaphase. Images are max projection of cortical GFP:: $\beta$ -tubulin for  
20 60 frames (42 sec). Yellow and Magenta arrows indicate the MT dots whose  
21 residence time was shorter and longer than 2.1 sec, respectively. See also Video 3, 5-7.  
22 (D) Distribution of quantified cortical MT or EB1 residence time in wild-type animals.  
23 (E) Mean cortical MT residence time of indicated genotypes.  $n = 47, 42, 77, 67, 64,$   
24  $61, 37, 44$ , from left to right. Error bars show 95% CI. Double asterisk and asterisk

1 indicate:  $p < 0.01$  and  $p < 0.05$  compared to control (Kruskal-Wallis test followed by  
2 Dunn's multiple comparison test).

3

4 **Figure 4 APR-1 asymmetrically attenuates pulling forces acting on the mitotic**  
5 **spindle.**

6 (A) Spindle severing experiments. The midzones of mitotic spindles were severed by  
7 laser irradiation around anaphase onset (upper left panel). Upon spindle severing,  
8 spindle remnants moved at different velocities depending on the net strength of  
9 pulling forces (upper right panel). Montages of dissected spindle dynamics were  
10 shown in the bottom panels as DIC images; spindle poles devoid of yolk granules  
11 were indicated by arrowheads. (B) Average peak velocity of spindle poles after  
12 spindle severing. (C) The average of outward pulling forces over 5 sec from anaphase  
13 onset ( $t = 100$  s) for 20 independent simulations. Error bars show 95% CI. Double  
14 asterisk and asterisk indicate:  $p < 0.01$  and  $p < 0.05$  compared to control (one-way  
15 ANOVA with Holm-Sidak's method). (D) Summary of relationships between cortical  
16 APR-1 level, cortical MT residence, cortical MT catastrophe frequencies, and spindle  
17 pulling forces.

18

19 **Figure 5 Anterior APR-1 and LIN-5 phosphorylation together attenuate spindle**  
20 **pulling forces to generate pulling force asymmetry.**

21 (A) Average peak velocity of spindle poles after spindle severing. Error bars show  
22 95% CI. Double asterisk and asterisk indicate:  $p < 0.01$  and  $p < 0.05$  compared to  
23 control (one-way ANOVA with Holm-Sidak's method). (B) Three elementary  
24 processes used in the model described in the panel C. (1) aPKC-dependent LIN-5  
25 phosphorylation results in the inhibition of force generation, (2) Cortical MT

1 stabilization by APC reduces the MT catastrophe frequency and (3) MT shrinkage-  
2 dependent force generation is suppressed by step (2). (C) A schematic model of  
3 asymmetric spindle force regulation in P0 cell (see text). (D) A diagram of spindle  
4 pulling force regulation pathways at the anterior cell cortex.

5

6 **Figure S1. Numbers of GFP::APR-1 dots in different cell cycle stages.**

7 Quantified numbers of GFP::APR-1 dots on the anterior and posterior cell cortex are  
8 shown for prophase, metaphase and anaphase and telophase of control and RNAi  
9 embryos. Ends of whiskers indicate minimum to maximum values. Double asterisk,  
10 asterisk and n.s. indicates:  $p < 0.01$ ,  $p < 0.05$  and  $p > 0.05$  (One-way ANOVA with  
11 Holm-Sidak's multiple comparison test).

12

13 **Figure S2. Roles of Wnt signaling in APR-1 localization.**

14 (A, B) Cell-surface GFP::APR-1 localization in RNAi of *dsh-2; mig-5*/dishevelled and  
15 *wrm-1*/β-catenin embryos. (C) Quantified GFP::APR-1 signal intensity per area of the  
16 whole embryo including the cell cortex and cytoplasm. (D) Immunofluorescence  
17 images of the DSH-2 protein during P0 and EMS cell division. Blue is DAPI staining.  
18 In EMS, the DSH-2 protein is enriched at the cell boundary between EMS and P2  
19 (arrowheads) while no asymmetry was observed in P0. (E) Localizations of the cell  
20 fate determinant GFP::PIE-1 in the indicated genotypes. Control and *apr-1(RNAi)*  
21 shows PIE-1 enrichment in the posterior blastomere P1. In the *par-2* mutant, PIE-1  
22 asymmetry was lost.

23

24 **Figure S3. Effects of *mom-5(RNAi)* on spindle pole movements and embryo sizes.**

1 (A) Kymographs of the spindle movements in *mom-5(RNAi)*. Kymographs were  
2 generated as in Figure 2. (B) Distance traveled by the anterior or posterior spindle  
3 poles. Total distance centrosome traveled for  $\pm 40$  sec and  $\pm 100$  sec of anaphase  
4 onset were shown for real embryos (left) and 3D simulations (right). (B) Cell volume  
5 of RNAi-treated embryos. Error bars show 95% CI. Asterisk indicate  $p < 0.05$   
6 compared to control (Kruskal-Wallis test followed by Dunn's multiple comparison  
7 test).

8

9 **Figure S4. Estimation of catastrophe frequencies at the cortex.**

10 (A) Frequencies of MT residence times at the cell cortex observed experimentally  
11 (histograms) and predicted from the estimated catastrophe frequencies (black lines).  
12 (B) Estimated catastrophe frequencies for indicated genotypes. The data is the same  
13 as in Supplementary Table 1.

14

15

16 **Figure S5. Numerical simulation of spindle movements**

17 (A-D) Representative trajectories of the spindle poles in the simulation. The  
18 trajectories of the anterior (green) and posterior (red) poles are shown. Their midpoint  
19 (black) is also shown in (A and D). (A, B) Control condition. (C, D) *apr-1 (RNAi)*  
20 condition. (A and D) Trajectories along A-P axis (x axis). (C and E) and those along  
21 an axis perpendicular to the x axis (y axis) are shown.

22

23

24 **Table 1. Estimated catastrophe frequencies of the microtubules at the cortex.**

25 When catastrophe occurs stochastically with the frequency of  $\lambda$ , the probability

1 distribution of the cortical residency time will be  $P(t) = \lambda \exp(-\lambda t)$ . Therefore, the  
2 probability of observing cortical residency time between  $t_1$  and  $t_2$  will be  $P(t_1 \sim t_2) =$   
3  $\exp(-\lambda t_1) - \exp(-\lambda t_2)$ . We fitted the experimentally obtained probability distribution of  
4 the cortical MT residency time to this equation to estimate the catastrophe frequencies  
5 of the MTs at the cortex.

6

7 **Table 2. Parameter values used in the simulation.**

8

9 **Video 1. Spindle movements in a control embryo.**

10 An embryo expressing GFP-histone H2B and GFP- $\beta$ -tubulin is shown from  
11 metaphase to telophase

12

13 **Video 2. Spindle movements in an *apr-1(RNAi)* embryo.**

14 An embryo expressing GFP-histone H2B and GFP- $\beta$ -tubulin is shown from  
15 metaphase to telophase

16

17 **Video 3.  $\beta$ -tubulin localization at the cell cortex in a control embryo.**

18 An embryo expressing GFP-histone H2B and GFP- $\beta$ -tubulin is shown for 42 sec from  
19 metaphase to anaphase (judged by the chromosome) with 700 msec intervals. Yellow  
20 and Magenta arrows indicate the MT dots whose residence times were shorter and  
21 longer than 2.1 sec.

22

23 **Video 4. Simultaneous imaging of tubulin and EB1 localization in a control**  
24 **embryo.**

1 Anaphase GFP- $\beta$ -tubulin and EB1-mKate2 at the cell surface (upper panels) and in  
2 the midplane (bottom panels) were shown. Blue arrowheads in the bottom indicate  
3 two bundled MTs with multiple EB1 foci.

4

5 **Video 5.  $\beta$ -tubulin localization at the cell cortex in an *apr-1(RNAi)* embryo.**

6 An embryo expressing GFP-histone H2B and GFP- $\beta$ -tubulin is shown for 42 sec from  
7 metaphase to anaphase (judged by the chromosomes) with 700 msec intervals. Yellow  
8 and Magenta arrows indicate the MT dots whose residence times were shorter and  
9 longer than 2.1 sec.

10

11 **Video 6.  $\beta$ -tubulin localization at the cell cortex in a *mom-5(null)* embryo.**

12 An embryo expressing GFP-histone H2B and GFP- $\beta$ -tubulin is shown for 42 sec from  
13 metaphase to anaphase (judged by the chromosomes) with 700 msec intervals. Yellow  
14 and Magenta arrows indicate the MT dots whose residence times were shorter and  
15 longer than 2.1 sec.

16

17 **Video 7.  $\beta$ -tubulin localization at the cell cortex in an *apr-1(RNAi); mom-5(null)*  
18 **embryo.****

19 An embryo expressing GFP-histone H2B and GFP- $\beta$ -tubulin is shown for 42 sec from  
20 metaphase to anaphase (judged by the chromosomes) with 700 msec intervals. Yellow  
21 and Magenta arrows indicate the MT dots whose residence times were shorter and  
22 longer than 2.1 sec.

23

24 **Video 8. Spindle severing experiments.**

- 1 A DIC movies of indicated embryos during spindle severing experiments. Spindle
- 2 was irradiated by a laser when the chromosomes appeared to be separated (anaphase
- 3 onset).
- 4 **Video 9. An example of 3D simulation.**

## 1   **References**

2

- 3   1.    Bahmanyar, S., Nelson, W.J. & Barth, A.I. Role of APC and its binding  
4       partners in regulating microtubules in mitosis. *Advances in experimental*  
5       *medicine and biology* **656**, 65-74 (2009).
- 6   2.    Barth, A.I., Caro-Gonzalez, H.Y. & Nelson, W.J. Role of adenomatous  
7       polyposis coli (APC) and microtubules in directional cell migration and  
8       neuronal polarization. *Semin Cell Dev Biol* **19**, 245-251 (2008). doi:  
9       10.1016/j.semcdb.2008.02.003.
- 10  3.    Beamish, H., de Boer, L., Giles, N., Stevens, F., Oakes, V., and Gabrielli, B.  
11       Cyclin A/cdk2 regulates adenomatous polyposis coli-dependent mitotic  
12       spindle anchoring. *J Biol Chem* **284**, 29015-29023 (2009). doi:  
13       10.1074/jbc.M109.042820.
- 14  4.    Berends, C. W. H., Munoz, J., Portegijs, V., Schmidt, R., Grigoriev, I., Boxem,  
15       M., Akhmanova, A., Heck, A. J. R. & van den Heuvel, S. F-actin asymmetry  
16       and the endoplasmic reticulum-associated TCC-1 protein contribute to  
17       stereotypic spindle movements in the *Caenorhabditis elegans* embryo. *Mol.*  
18       *Biol. Cell* **24**, 2201–2215 (2013).
- 19  5.    Brenner, S. The genetics of *Caenorhabditis elegans*. *Genetics* **77**, 71-94  
20       (1974).
- 21  6.    Cheeseman, I.M., MacLeod, I., Yates, J.R., Oegema, K. & Desai, A. The  
22       CENP-F-like proteins HCP-1 and HCP-2 target CLASP to kinetochores to  
23       mediate chromosome segregation. *Curr Biol* **15**, 771-777 (2005).
- 24  7.    Clevers, H. & Nusse, R. Wnt/beta-catenin signaling and disease. *Cell* **149**,  
25       1192-1205 (2012). doi: 10.1016/j.cell.2012.05.012.

- 1 8. Dickinson, D.J., Ward, J.D., Reiner, D.J., & Goldstein, B. Engineering the  
2 *Caenorhabditis elegans* genome using Cas9-triggered homologous  
3 recombination. *Nat. Methods* **10**, 1028-1034. (2013)
- 4 9. di Pietro, F., Echard, A. & Morin, X. Regulation of mitotic spindle orientation:  
5 an integrated view. *EMBO Rep.* **17**, 1106–1130. (2016)
- 6 10. Edgar, L.G. Blastomere culture and analysis. *Methods Cell Biol* **48**, 303-321  
7 (1995).
- 8 11. Etienne-Manneville, S. APC in cell migration. *Advances in experimental*  
9 *medicine and biology* **656**, 30-40 (2009).
- 10 12. Etienne-Manneville, S. & Hall, A. Cdc42 regulates GSK-3 $\beta$  and adenomatous  
11 polyposis coli to control cell polarity. *Cell* **421**, 753-756 (2003).
- 12 13. Fodde, R., Kuipers, J., Rosenberg, C., Smits, R., Kielman, M., Gaspar, C., van  
13 Es, J.H., Breukel, C., Wiegant, J., Giles, R.H., Clevers, H.. Mutations in the  
14 APC tumour suppressor gene cause chromosomal instability. *Nat Cell Biol* **3**,  
15 433-438 (2001).
- 16 14. Friedland, A.E., Tzur, Y.B., Esvelt, K.M., Colaiacovo, M.P., Church, G.M.,  
17 and Calarco, J.A. Heritable genome editing in *C. elegans* via a CRISPR-  
18 Cas9 system. *Nat Methods* **10**, 741-743 (2013). doi: 10.1038/nmeth.2532.
- 19 15. Galli, M., Munoz, J., Portegijs, V., Boxem, M., Grill, S.W., Heck, A.J., and  
20 van den Heuvel, S. aPKC phosphorylates NuMA-related LIN-5 to position  
21 the mitotic spindle during asymmetric division. *Nat Cell Biol* **13**, 1132-1138  
22 (2011). doi: 10.1038/ncb2315.
- 23 16. Galli, M. & van den Heuvel, S. Determination of the cleavage plane in early *C.*  
24 *elegans* embryos. *Annu Rev Genet* **42**, 389-411 (2008). doi:  
25 10.1146/annurev.genet.40.110405.090523.

- 1 17. Garzon-Coral, H., Fantana, H. A. & Howard, J. A force-generating machinery  
2 maintains the spindle at the cell center during mitosis. *Science* **352**, 1124-  
3 1127. (2016).
- 4 18. Gibson, D.G., Young, L., Chuang, R.Y., Venter, J.C., Hutchison, C.A., 3rd, &  
5 Smith, H.O. Enzymatic assembly of DNA molecules up to several hundred  
6 kilobases. *Nat Methods* **6**, 343-345. (2009).
- 7 19. Gönczy, P. Mechanisms of asymmetric cell division: flies and worms pave the  
8 way. *Nat Rev Mol Cell Biol* **9**, 355-366 (2008). doi: 10.1038/nrm2388.
- 9 20. Green, R.A. & Kaplan, K.B. Chromosome instability in colorectal tumor cells  
10 is associated with defects in microtubule plus-end attachments caused by a  
11 dominant mutation in APC. *J Cell Biol* **163**, 949-961 (2003).
- 12 21. Green, R.A., Wollman, R. & Kaplan, K.B. APC and EB1 function together in  
13 mitosis to regulate spindle dynamics and chromosome alignment. *Mol Biol*  
14 *Cell* **16**, 4609-4622 (2005).
- 15 22. Grill, S., Kruse, K. & Jülicher, F. Theory of Mitotic Spindle Oscillations. *Phys*  
16 *Rev Lett* **94**, 1-4 (2005).
- 17 23. Grill, S.W., Gönczy, P., Stelzer, E.H. & Hyman, A.A. Polarity controls forces  
18 governing asymmetric spindle positioning in the *Caenorhabditis elegans*  
19 embryo. *Nature* **409**, 630-633 (2001).
- 20 24. Grill, S.W., Howard, J., Schäffer, E., Stelzer, E.H.K. & Hyman, A.A. The  
21 distribution of active force generators controls mitotic spindle position.  
22 *Science* **301**, 518-521 (2003).
- 23 25. Gundersen, G., Gomes, E. & Wen, Y. Cortical control of microtubule stability  
24 and polarization. *Curr Opin Cell Biol* **16**, 106-112 (2004). doi:  
25 10.1016/j.ceb.2003.11.010.

- 1
- 2 26. Habib, S.J., Chen, B.C., Tsai, F.C., Anastassiadis, K., Meyer, T., Betzig, E.,  
3 and Nusse, R. A localized Wnt signal orients asymmetric stem cell division in  
4 vitro. *Science* **339**, 1445-1448 (2013). doi: 10.1126/science.1231077.
- 5 27. Hamaguchi, M.S. & Hiramoto, Y. Analysis of the Role of Astral Rays in  
6 Pronuclear Migration in Sand Dollar Eggs by the Colcemid - UV Method.  
7 *Dev Growth Differ* **28**, 143-156 (1986).
- 8 28. Hanahan, D. & Weinberg, R.A. Hallmarks of cancer: the next generation. *Cell*  
9 **144**, 646-674 (2011). doi: 10.1016/j.cell.2011.02.013.
- 10 29. Hara, Y. & Kimura, A. Cell-size-dependent spindle elongation in the  
11 *Caenorhabditis elegans* early embryo. *Curr Biol* **19**, 1549-1554 (2009). doi:  
12 10.1016/j.cub.2009.07.050.
- 13 30. Harterink, M., Kim, D.H., Middelkoop, T.C., Doan, T.D., van Oudenaarden,  
14 A., and Korswagen, H.C. Neuroblast migration along the anteroposterior axis  
15 of *C. elegans* is controlled by opposing gradients of Wnts and a secreted  
16 Frizzled-related protein. *Development* **138**, 2915-2924 (2011). doi:  
17 10.1242/dev.064733.
- 18 31. Hawkins, N.C., Ellis, G.C., Bowerman, B. & Garriga, G. MOM-5 frizzled  
19 regulates the distribution of DSH-2 to control *C. elegans* asymmetric  
20 neuroblast divisions. *Dev Biol* **284**, 246-259 (2005).
- 21 32. Hwang, E., Kusch, J., Barral, Y. & Huffaker, T.C. Spindle orientation in  
22 *Saccharomyces cerevisiae* depends on the transport of microtubule ends along  
23 polarized actin cables. *J Cell Biol* **161**, 483-488 (2003).

- 1 33. Kaplan, K.B., Burds, a.a., Swedlow, J.R., Bekir, S.S., Sorger, P.K., and  
2 N athke, I.S. A role for the Adenomatous Polyposis Coli protein in  
3 chromosome segregation. *Nat Cell Biol* **3**, 429-432 (2001).
- 4 34. Kimura, A. & Onami, S. Computer simulations and image processing reveal  
5 length-dependent pulling force as the primary mechanism for *C. elegans* male  
6 pronuclear migration. *Dev Cell* **8**, 765-775 (2005).
- 7 35. Kimura, A. & Onami, S. Local cortical pulling-force repression switches  
8 centrosomal centration and posterior displacement in *C. elegans*. *J Cell Biol*  
9 **179**, 1347-1354 (2007).
- 10 36. Kimura, A. & Onami, S. Modeling microtubule-mediated forces and  
11 centrosome positioning in *Caenorhabditis elegans* embryos. *Methods Cell*  
12 *Biol* **97**, 437-453 (2010). doi: 10.1016/S0091-679X(10)97023-4.
- 13 37. Kimura, K. & Kimura, A. Intracellular organelles mediate cytoplasmic pulling  
14 force for centrosome centration in the *Caenorhabditis elegans* early embryo.  
15 *Proc Natl Acad Sci U S A* **108**, 137-142 (2011). doi:  
16 10.1073/pnas.1013275108.
- 17 38. Kiyomitsu, T. & Cheeseman, I.M. Chromosome- and spindle-pole-derived  
18 signals generate an intrinsic code for spindle position and orientation. *Nat Cell*  
19 *Biol* **14**, 311-317 (2012). doi: 10.1038/ncb2440.
- 20 39. Knoblich, J. Asymmetric cell division: recent developments and their  
21 implications for tumour biology. *Nat Rev Mol Cell Biol* **11**, 849-860 (2010).  
22 doi: 10.1038/nrm3010.  
23

- 1 40. Korinek, W.S., Copeland, M.J., Chaudhuri, A. & Chant, J. Molecular linkage  
2 underlying microtubule orientation toward cortical sites in yeast. *Science* **287**,  
3 2257-2259 (2000).
- 4 41. Kozlowski, C., Srayko, M. & Nedelec, F. Cortical microtubule contacts  
5 position the spindle in *C. elegans* embryos. *Cell* **129**, 499-510 (2007).
- 6 42. Krueger, L., Wu, J., Tsou, M. & Rose, L. LET-99 inhibits lateral posterior  
7 pulling forces during asymmetric spindle elongation in *C. elegans* embryos. *J*  
8 *Cell Biol* **189**, 481-495 (2010). doi: 10.1083/jcb.201001115.
- 9 43. Laan, L., Pavin, N., Husson, J., Romet-Lemonne, G., van Duijn, M., Lopez,  
10 M.P., Vale, R.D., Julicher, F., Reck-Peterson, S.L., and Dogterom, M. Cortical  
11 dynein controls microtubule dynamics to generate pulling forces that position  
12 microtubule asters. *Cell* **148**, 502-514 (2012). doi: 10.1016/j.cell.2012.01.007.
- 13 44. Labbé, J.C., Maddox, P.S., Salmon, E.D. & Goldstein, B. PAR proteins  
14 regulate microtubule dynamics at the cell cortex in *C. elegans*. *Curr Biol* **13**,  
15 707-714 (2003).
- 16 45. Lee, L., Tirnauer, J.S., Li, J., Schuyler, S.C., Liu, J.Y., and Pellman, D.  
17 Positioning of the mitotic spindle by a cortical-microtubule capture  
18 mechanism. *Science* **287**, 2260-2262 (2000).
- 19 46. McCartney, B.M., McEwen, D.G., Grevengoed, E., Maddox, P., Bejsovec, a.,  
20 and Peifer, M. *Drosophila* APC2 and Armadillo participate in tethering  
21 mitotic spindles to cortical actin. *Nat Cell Biol* **3**, 933-938 (2001).
- 22 47. Merritt, C., Rasoloson, D., Ko, D. & Seydoux, G. 3' UTRs are the primary  
23 regulators of gene expression in the *C. elegans* germline. *Curr Biol* **18**, 1476-  
24 1482 (2008). doi: 10.1016/j.cub.2008.08.013.

- 1 48. Miller, R.K. & Rose, M.D. Kar9p is a novel cortical protein required for  
2 cytoplasmic microtubule orientation in yeast. *J Cell Biol* **140**, 377-390 (1998).
- 3 49. Mizumoto, K. & Sawa, H. Cortical beta-catenin and APC regulate asymmetric  
4 nuclear beta-catenin localization during asymmetric cell division in *C. elegans*.  
5 *Devl Cell* **12**, 287-299 (2007).
- 6 50. Moser, A.R., Dove, W.F., Roth, K.A. & Gordon, J.I. The Min (multiple  
7 intestinal neoplasia) mutation: its effect on gut epithelial cell differentiation  
8 and interaction with a modifier system. *J Cell Biol* **116**, 1517-1526 (1992).
- 9 51. Munro, E. & Bowerman, B. Cellular symmetry breaking during  
10 *Caenorhabditis elegans* development. *Cold Spring Harb Perspect Biol* **1**,  
11 a003400 (2009). doi: 10.1101/cshperspect.a003400.
- 12 52. Nelson, S. & Näthke, I.S. Interactions and functions of the adenomatous  
13 polyposis coli (APC) protein at a glance. *J Cell Sci* **126**, 873-877 (2013). doi:  
14 10.1242/jcs.100479.
- 15 53. Nguyen-Ngoc, T., Afshar, K. & Gönczy, P. Coupling of cortical dynein and G  
16 alpha proteins mediates spindle positioning in *Caenorhabditis elegans*. *Nat*  
17 *Cell Biol* **9**, 1294-1302 (2007).
- 18 54. Oldenbroek, M., Robertson, S.M., Guven-Ozkan, T., Spike, C., Greenstein, D.,  
19 and Lin, R. Regulation of maternal Wnt mRNA translation in *C. elegans*  
20 embryos. *Development* **140**, 4614-4623 (2013). doi: 10.1242/dev.096313.
- 21 55. Pecreaux, J., Röper, J.-C., Kruse, K., Jülicher, F., Hyman, A.a., Grill, S.W.,  
22 and Howard, J. Spindle oscillations during asymmetric cell division require a  
23 threshold number of active cortical force generators. *Curr Biol* **16**, 2111-2122  
24 (2006).

- 1 56. Pereira, G. & Yamashita, Y.M. Fly meets yeast: checking the correct  
2 orientation of cell division. *Trends Cell Biol* **21**, 526-533 (2011). doi:  
3 10.1016/j.tcb.2011.05.004.
- 4 57. Portegijs, V., Fielmich, L. E., Galli, M., Schmidt, R., Muñoz, J., van Mourik,  
5 T., Akhmanova, A., Heck, A. J. R., Boxem, M. & van den Heuvel, S..  
6 Multisite phosphorylation of NuMA-related LIN-5 controls mitotic spindle  
7 positioning in *C. elegans*. *PLoS Genet.* **12**, e1006291 (2016).  
8 doi:10.1371/journal.pgen.1006291
- 9 58. Poulton, J.S., Mu, F.W., Roberts, D.M. & Peifer, M. APC2 and Axin promote  
10 mitotic fidelity by facilitating centrosome separation and cytoskeletal  
11 regulation. *Development* **140**, 4226-4236 (2013). doi: 10.1242/dev.094425.
- 12 59. Praitis, V., Casey, E., Collar, D. & Austin, J. Creation of low-copy integrated  
13 transgenic lines in *Caenorhabditis elegans*. *Genetics* **157**, 1217-1226 (2001).
- 14 60. Reilein, A. & Nelson, W.J. APC is a component of an organizing template for  
15 cortical microtubule networks. *Nat Cell Biol* **7**, 463-473 (2005).
- 16 61. Rose, L. & Gönczy, P. Polarity establishment, asymmetric division and  
17 segregation of fate determinants in early *C. elegans* embryos. (December 30,  
18 2014), *WormBook*, ed. The *C. elegans* Research Community, WormBook, doi:  
19 10.1895/wormbook.1.30.2
- 20 62. Rusan, N.M. & Peifer, M. Original CIN: reviewing roles for APC in  
21 chromosome instability. *J Cell Biol* **181**, 719-726 (2008). doi:  
22 10.1083/jcb.200802107.
- 23 63. Schlessinger, K., McManus, E. & Hall, A. Cdc42 and noncanonical Wnt  
24 signal transduction pathways cooperate to promote cell polarity. *J Cell Biol*  
25 **178**, 355-361 (2007). doi: 10.1083/jcb.200701083.

- 1 64. Schmidt, R., Akhmanova, A.A., and van den Heuvel, S.J.L. Normal spindle  
2 positioning in the absence of EBPs and dynein plus-end tracking in *C. elegans*.  
3 *bioRxiv* 118935 (2017). doi:10.1101/118935
- 4 65. Schneider, C.A., Rasband, W.S. & Eliceiri, K.W. NIH Image to ImageJ: 25  
5 years of image analysis. *Nat Methods* **9**, 671-675 (2012).
- 6 66. Siller, K.H., Cabernard, C. & Doe, C.Q. The NuMA-related Mud protein  
7 binds Pins and regulates spindle orientation in *Drosophila* neuroblasts. *Nat*  
8 *Cell Biol* **8**, 594-600 (2006).
- 9 67. Siller, K.H. & Doe, C.Q. Spindle orientation during asymmetric cell division.  
10 *Nat Cell Biol* **11**, 365-374 (2009). doi: 10.1038/ncb0409-365.
- 11 68. Srinivasan, D.G., Fisk, R.M., Xu, H. & van den Heuvel, S. A complex of LIN-  
12 5 and GPR proteins regulates G protein signaling and spindle function in *C*  
13 *elegans*. *Genes Dev* **17**, 1225-1239 (2003).
- 14 69. Strome, S., Powers, J., Dunn, M., Reese, K., Malone, C.J., White, J., Seydoux,  
15 G., and Saxton, W. Spindle dynamics and the role of gamma-tubulin in early  
16 *Caenorhabditis elegans* embryos. *Mol Biol Cell* **12**, 1751-1764 (2001).
- 17 70. Su, L.K., Kinzler, K.W., Vogelstein, B., Preisinger, A.C., Moser, A.R.,  
18 Luongo, C., Gould, K.A., and Dove, W.F. Multiple intestinal neoplasia caused  
19 by a mutation in the murine homolog of the APC gene. *Science* **256**, 668-670  
20 (1992).
- 21 71. Sugioka, K., Mizumoto, K. & Sawa, H. Wnt regulates spindle asymmetry to  
22 generate asymmetric nuclear  $\beta$ -catenin in *C. elegans*. *Cell* **146**, 942-954  
23 (2011). doi: 10.1016/j.cell.2011.07.043.

- 1 72. Vogel, S.K., Pavin, N., Maghelli, N., Julicher, F. & Tolic-Norrelykke, I.M.  
2 Self-organization of dynein motors generates meiotic nuclear oscillations.  
3 *PLoS Biol* **7**, e1000087 (2009). doi: 10.1371/journal.pbio.1000087.
- 4 73. Walston, T., Tuskey, C., Edgar, L., Hawkins, N., Ellis, G., Bowerman, B.,  
5 Wood, W., and Hardin, J. Multiple Wnt signaling pathways converge to orient  
6 the mitotic spindle in early *C. elegans* embryos. *Dev Cell* **7**, 831-841 (2004).
- 7 74. Williams, S.E. & Fuchs, E. Oriented divisions, fate decisions. *Curr Opin Cell*  
8 *Biol* **25**, 749-758 (2013). doi: 10.1016/j.ceb.2013.08.003.
- 9 75. Yamashita, Y.M., Jones, D.L. & Fuller, M.T. Orientation of asymmetric stem  
10 cell division by the APC tumor suppressor and centrosome. *Science* **301**,  
11 1547-1550 (2003).
- 12 76. Zumbunn, J., Kinoshita, K., Hyman, A.A. & Näthke, I.S. Binding of the  
13 adenomatous polyposis coli protein to microtubules increases microtubule  
14 stability and is regulated by GSK3 beta phosphorylation. *Curr Biol* **11**, 44-49  
15 (2001).  
16  
17  
18

1	
2	<b>List of figures, tables and movies</b>
3	Figure 1-5
4	Table 1-2
5	Video 1-9
6	Figure S1
7	Figure S2
8	Figure S3
9	Figure S4
10	Figure S5

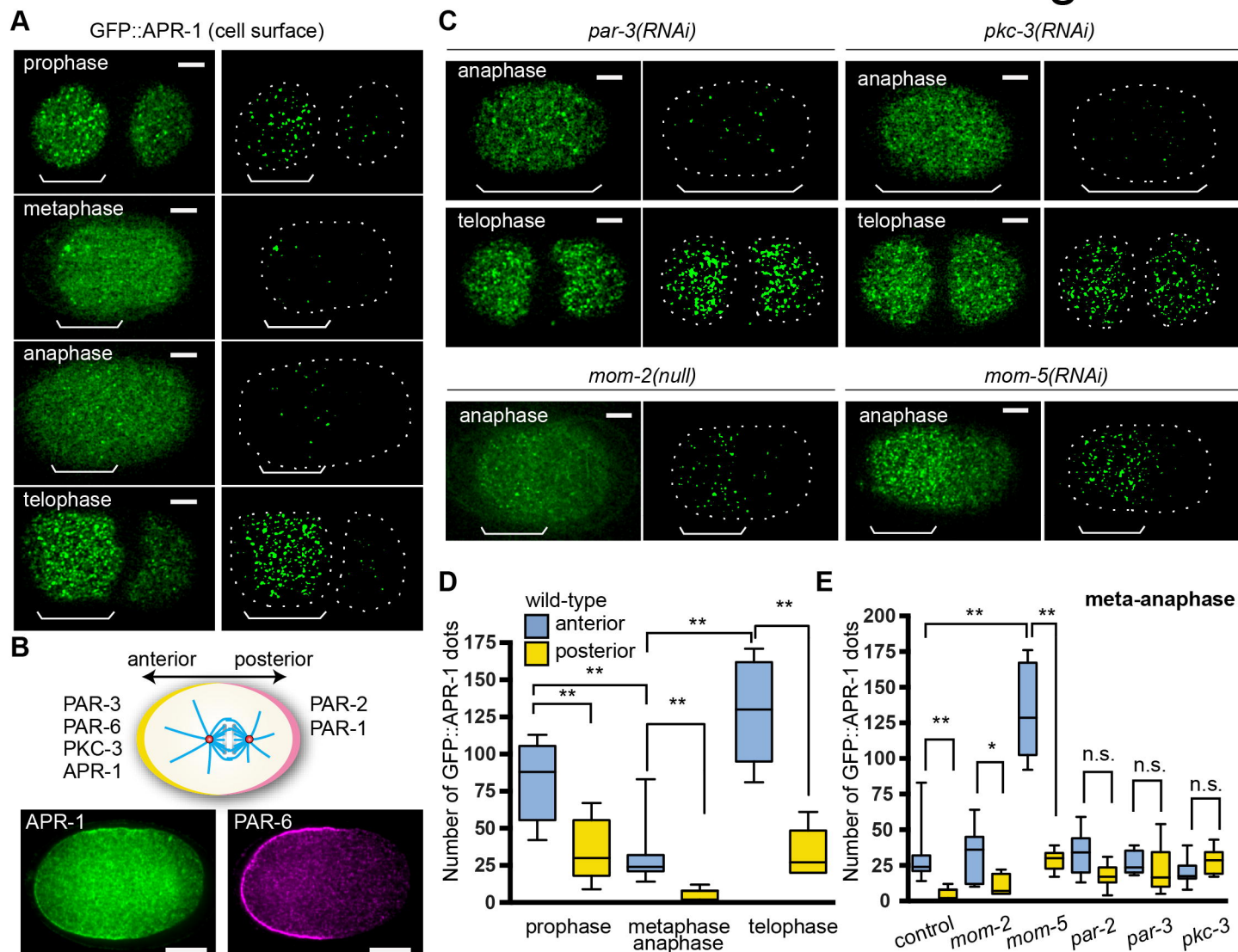


**Figure 1. The Par-aPKC system and Frizzled signaling regulate APR-1 asymmetric localization during zygote division.**

(A) GFP::*APR-1* signals on the cell surface in different cell cycle stages. In the right panels, computationally detected APR-1 dots were shown (see Material and Methods). (B) APR-1 and PAR-6 localizations in the cell midplane during asymmetric cell division. Schematic drawing shows polarized protein localizations. (C) GFP::*APR-1* signals on the cell surface in *mom-2(null)* mutants and *mom-5*, *par-2* or *par-3* RNAi embryos. (D) Quantified numbers of GFP::*APR-1* dots on the anterior and posterior cell cortex of wild-type embryos in different cell cycle stages.  $n = 5, 10, 5$  from left to right. (E) Quantified numbers of GFP::*APR-1* dots at metaphase or anaphase in RNAi embryos.  $n = 10, 7, 10, 9, 10, 10$ , from left to right. Ends of whiskers indicate minimum or maximum values. Double asterisk, asterisk and n.s. indicates:  $p < 0.01$ ,  $p < 0.05$  and  $p > 0.05$  (One-way ANOVA with Holm-Sidak's multiple comparison test). Scale bars are 10  $\mu\text{m}$ .

## Figure 2

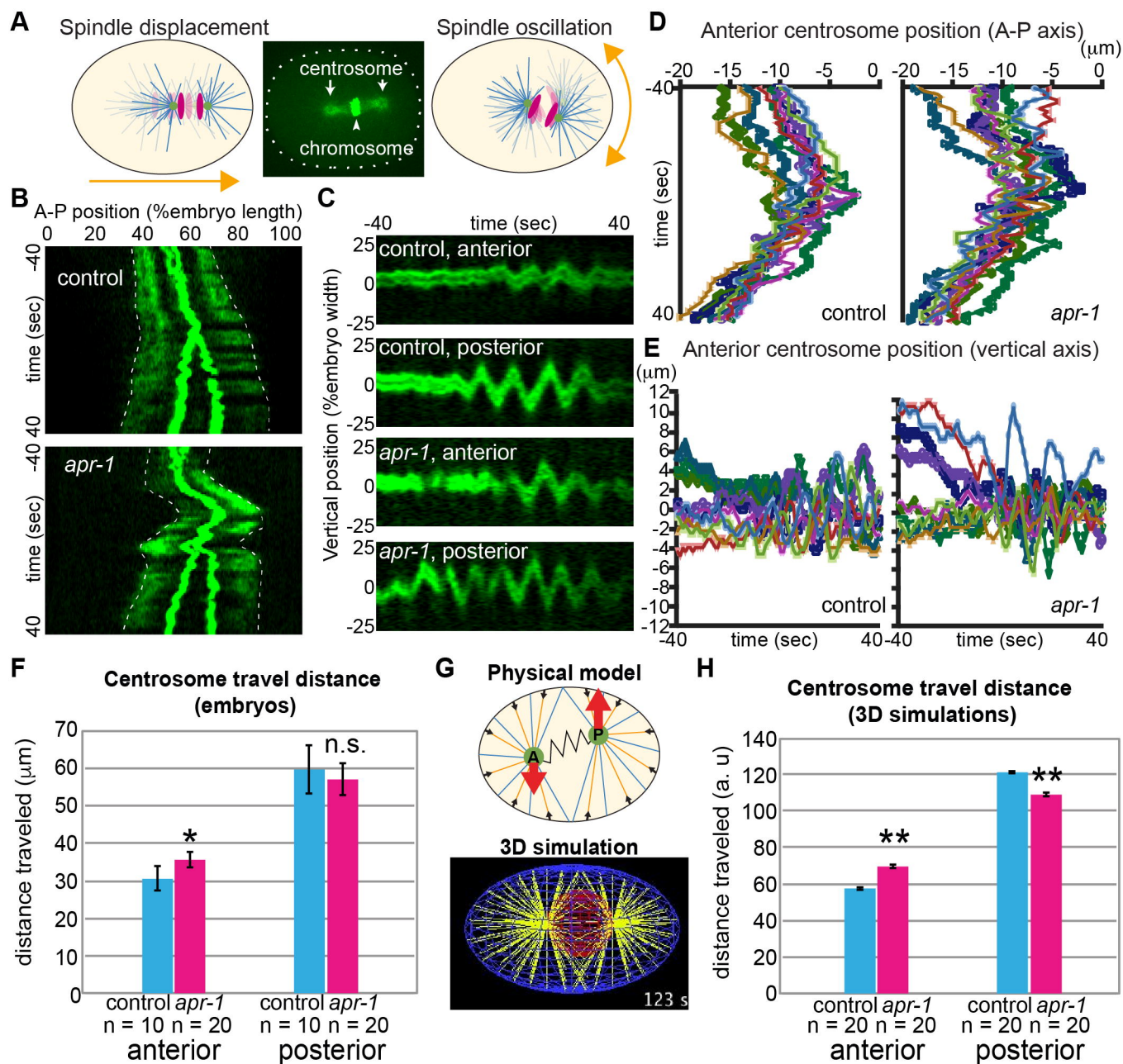


**Figure 2. APR-1 asymmetrically suppresses centrosome movements during the P0 cell division** (A) Schematic drawings of spindle movements along the A-P and transverse axes in fluorescent cells used to generate kymograph in B and C. (B) Kymograph of the spindle movement along the A-P axis. Weak signals outlined by dotted lines and strong signals in the center indicate the centrosomes and chromosomes, respectively. (C) Kymograph of the spindle movement along the transverse axis. (D, E) Trajectory of centrosome movements. Cell centers are zero in position. (F, H) Total distances for movements of the anterior and posterior poles in living embryo (F) and in 3D simulations (H). (G) Physical model used for 3D simulation. A and P indicate the anterior and posterior spindle poles harboring shrinking MTs (orange) and elongating MTs (blue). Red and black arrows indicate centrosome movements and cortical force generation. For each MT catastrophe at the cortex, the average pulling forces acting on single MT at the posterior are stronger than those at the anterior, due to the different probabilities of MT-force generator interactions (see Materials and methods). Times are  $\pm 40$  sec and  $\pm 100$  sec relative to the anaphase onset in living embryos and 3D simulations, respectively. Error bars show 95% CI. Double asterisk and n.s. indicates:  $p < 0.01$  and  $p > 0.05$  compared to control (Kruskal-Wallis test followed by Dunn's multiple comparison test).

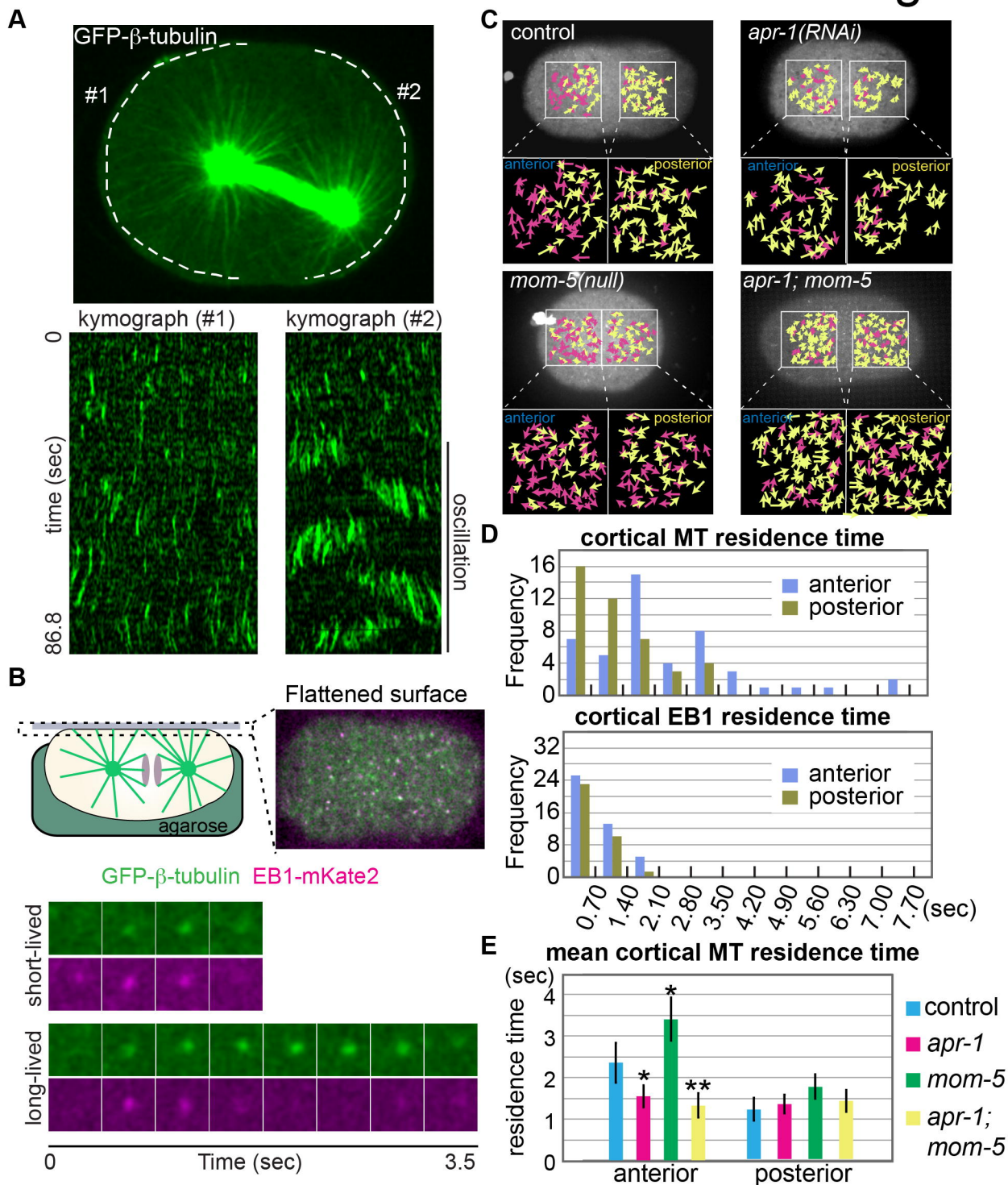


**Figure 3. APR-1 asymmetrically stabilizes microtubule-cortex interactions.**

(A) Kymographs of anterior and posterior cortical microtubules. Using the dotted lines #1 and #2, anterior and posterior kymographs were generated. (B) Measurement of cortical MT residence. The embryos were mounted on agarose pads and flattened by coverslips to visualize cortical microtubule ends in a single focal plane. Examples of short and long-lived foci were shown below with simultaneous imaging of GFP:: $\beta$ -tubulin and EB1::mKate2. (C) Cortical microtubule dots in the indicated genotypes during metaphase-anaphase. Images are max projection of cortical GFP:: $\beta$ -tubulin for 60 frames (42 sec). Yellow and Magenta arrows indicate the MT dots whose residence time was shorter and longer than 2.1 sec, respectively. See also Video 3, 5-7. (D) Distribution of quantified cortical MT or EB1 residence time in wild-type animals. (E) Mean cortical MT residence time of indicated genotypes.  $n = 47, 42, 77, 67, 64, 61, 37, 44$ , from left to right. Error bars show 95% CI. Double asterisk and asterisk indicate:  $p < 0.01$  and  $p < 0.05$  compared to control (Kruskal-Wallis test followed by Dunn's multiple comparison test).

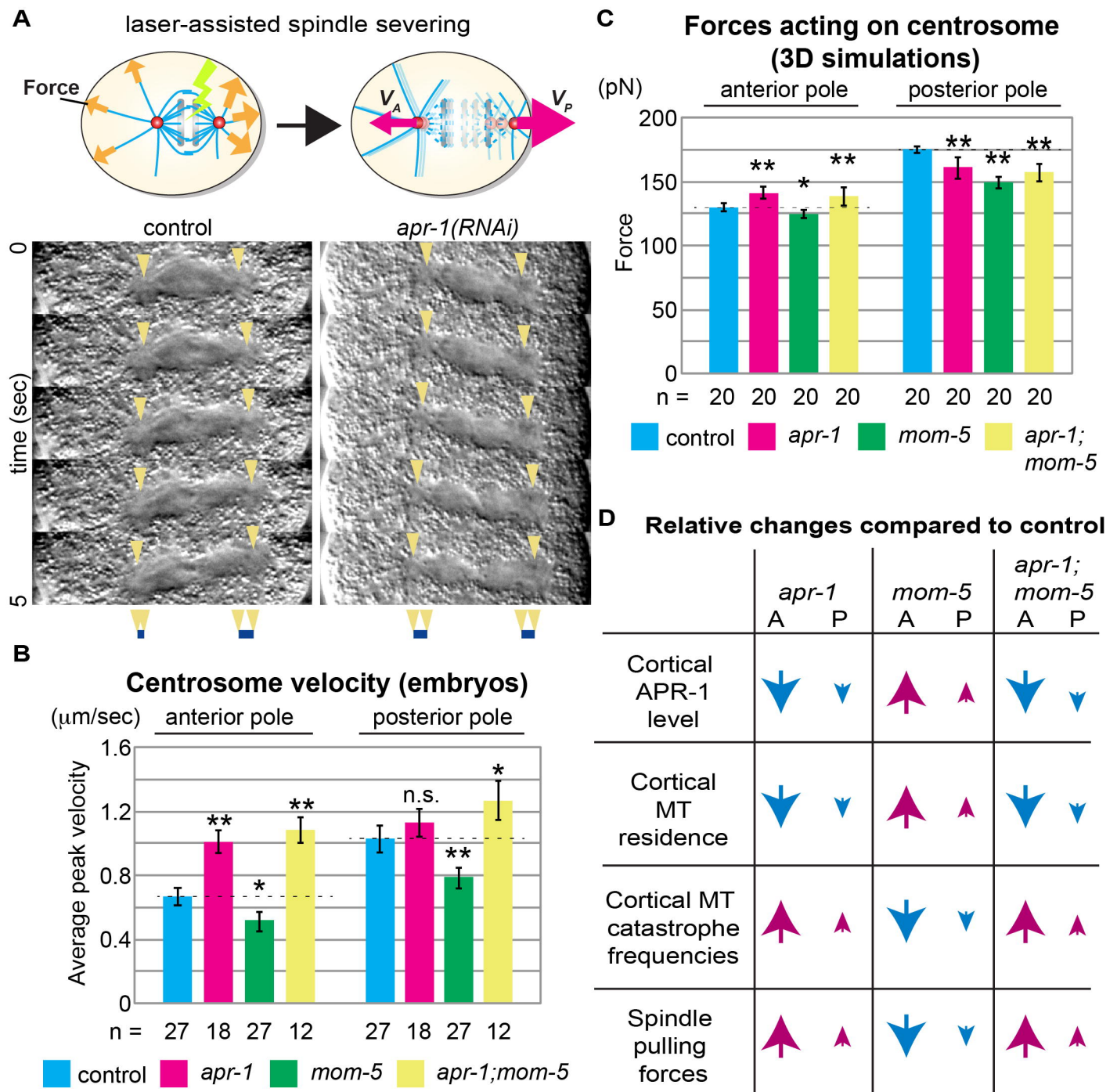


**Figure 4 APR-1 asymmetrically attenuates pulling forces acting on the mitotic spindle.**

(A) Spindle severing experiments. The midzones of mitotic spindles were severed by laser irradiation around anaphase onset (upper left panel). Upon spindle severing, spindle remnants moved at different velocities depending on the net strength of pulling forces (upper right panel). Montages of dissected spindle dynamics were shown in the bottom panels as DIC images; spindle poles devoid of yolk granules were indicated by arrowheads. (B) Average peak velocity of spindle poles after spindle severing. (C) The average of outward pulling forces over 5 sec from anaphase onset ( $t = 100$  s) for 20 independent simulations. Error bars show 95% CI. Double asterisk and asterisk indicate:  $p < 0.01$  and  $p < 0.05$  compared to control (one-way ANOVA with Holm-Sidak's method). (D) Summary of relationships between cortical APR-1 level, cortical MT residence, cortical MT catastrophe frequencies, and spindle pulling forces.

## Figure 5

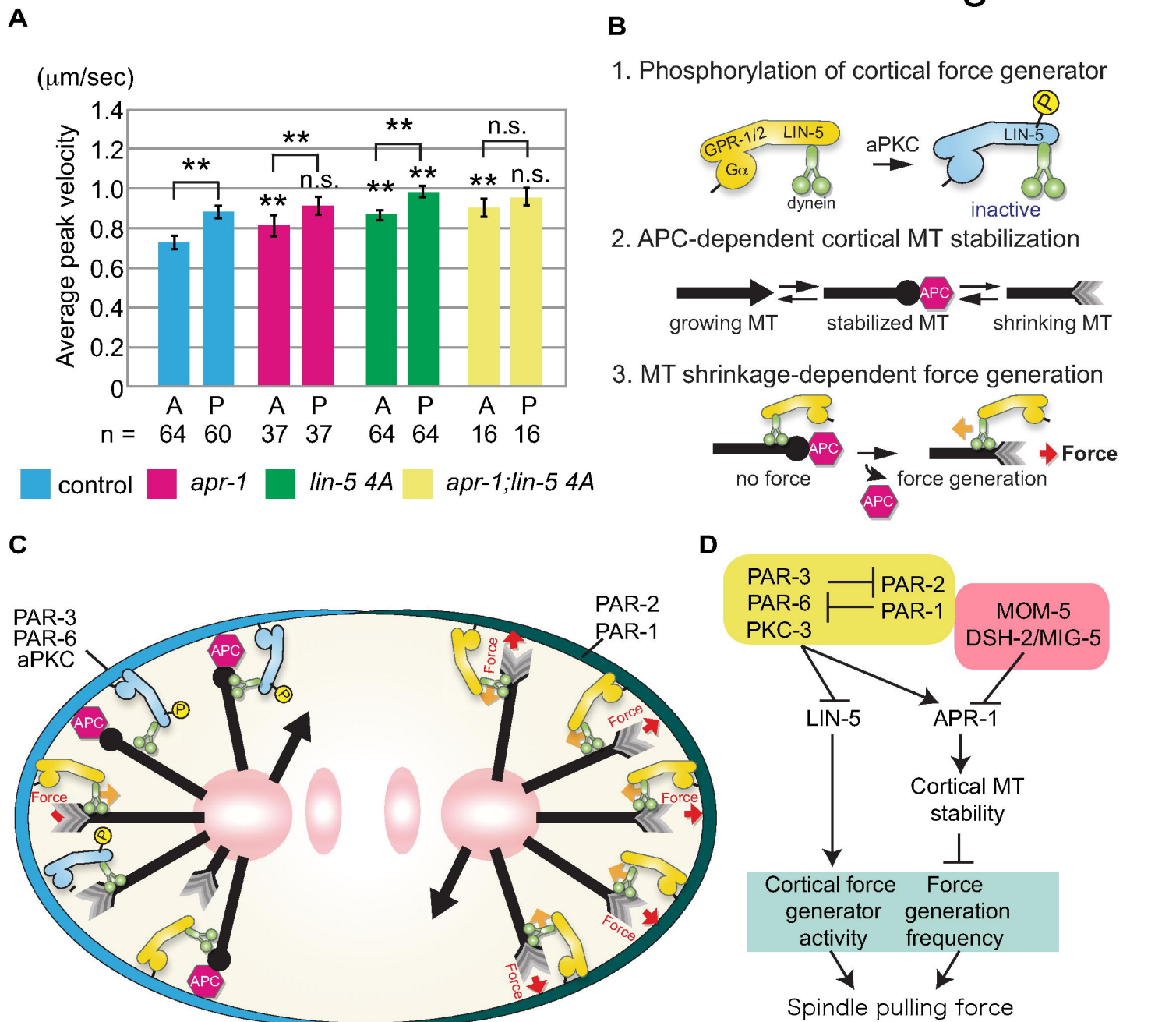


### Figure 5 Anterior APR-1 and LIN-5 phosphorylation together attenuate spindle pulling forces to generate pulling force asymmetry.

(A) Average peak velocity of spindle poles after spindle severing. Error bars show 95% CI. Double asterisk and asterisk indicate:  $p < 0.01$  and  $p < 0.05$  compared to control (one-way ANOVA with Holm-Sidak's method). (B) Three elementary processes used in the model described in the panel C. (1) aPKC-dependent LIN-5 phosphorylation results in the inhibition of force generation, (2) Cortical MT stabilization by APC reduces the MT catastrophe frequency and (3) MT shrinkage-dependent force generation is suppressed by step (2). (C) A schematic model of asymmetric spindle force regulation in P0 cell (see text). (D) A diagram of spindle pulling force regulation pathways at the anterior cell cortex.

# Figure S1

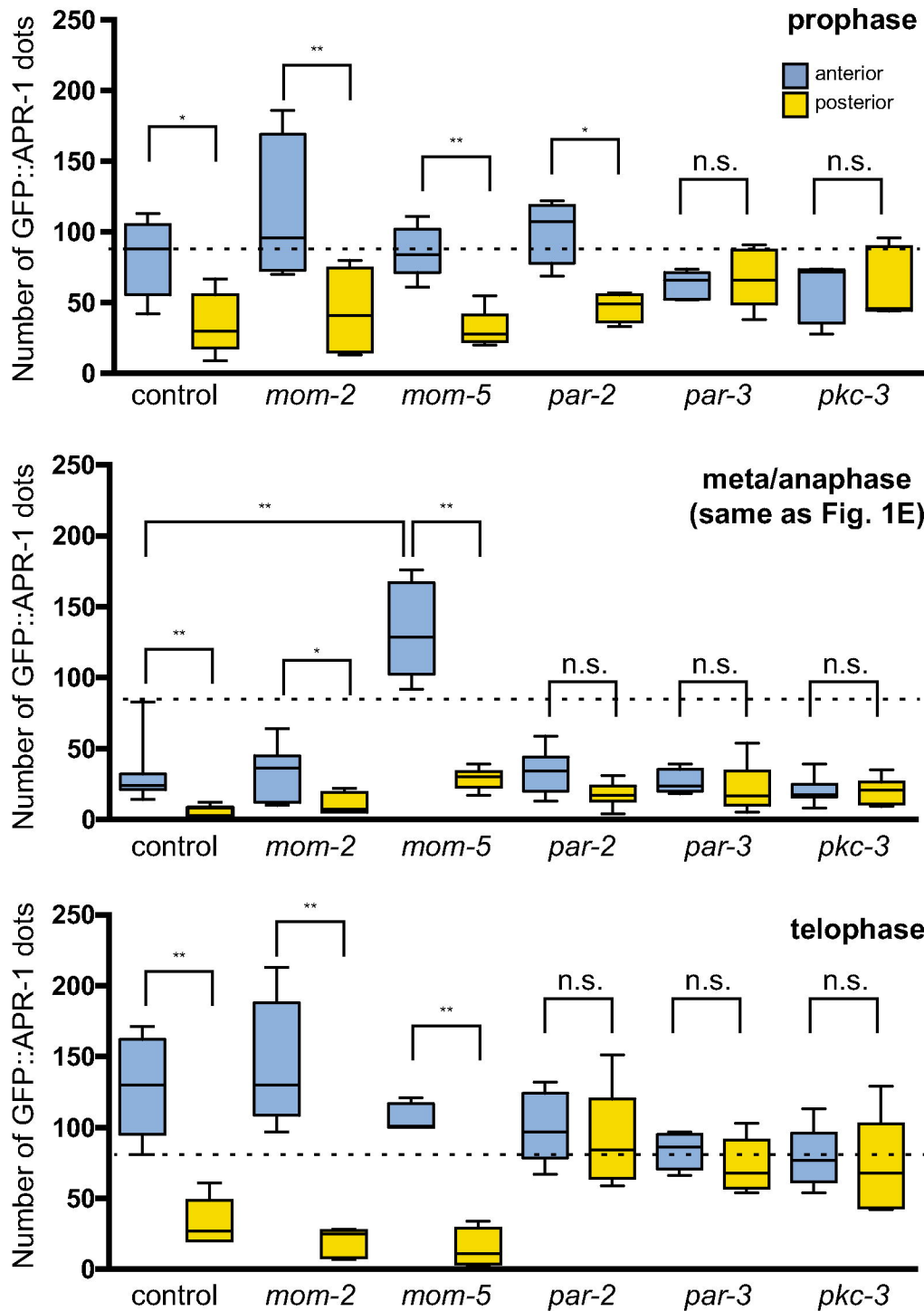


**Figure S1. Numbers of GFP::APR-1 dots in different cell cycle stages.**

Quantified numbers of GFP::APR-1 dots on the anterior and posterior cell cortex are shown for prophase, metaphase and anaphase and telophase of control and RNAi embryos. Ends of whiskers indicate minimum to maximum values. Double asterisk, asterisk and n.s. indicates:  $p < 0.01$ ,  $p < 0.05$  and  $p > 0.05$  (One-way ANOVA with Holm-Sidak's multiple comparison test).

## Figure S2

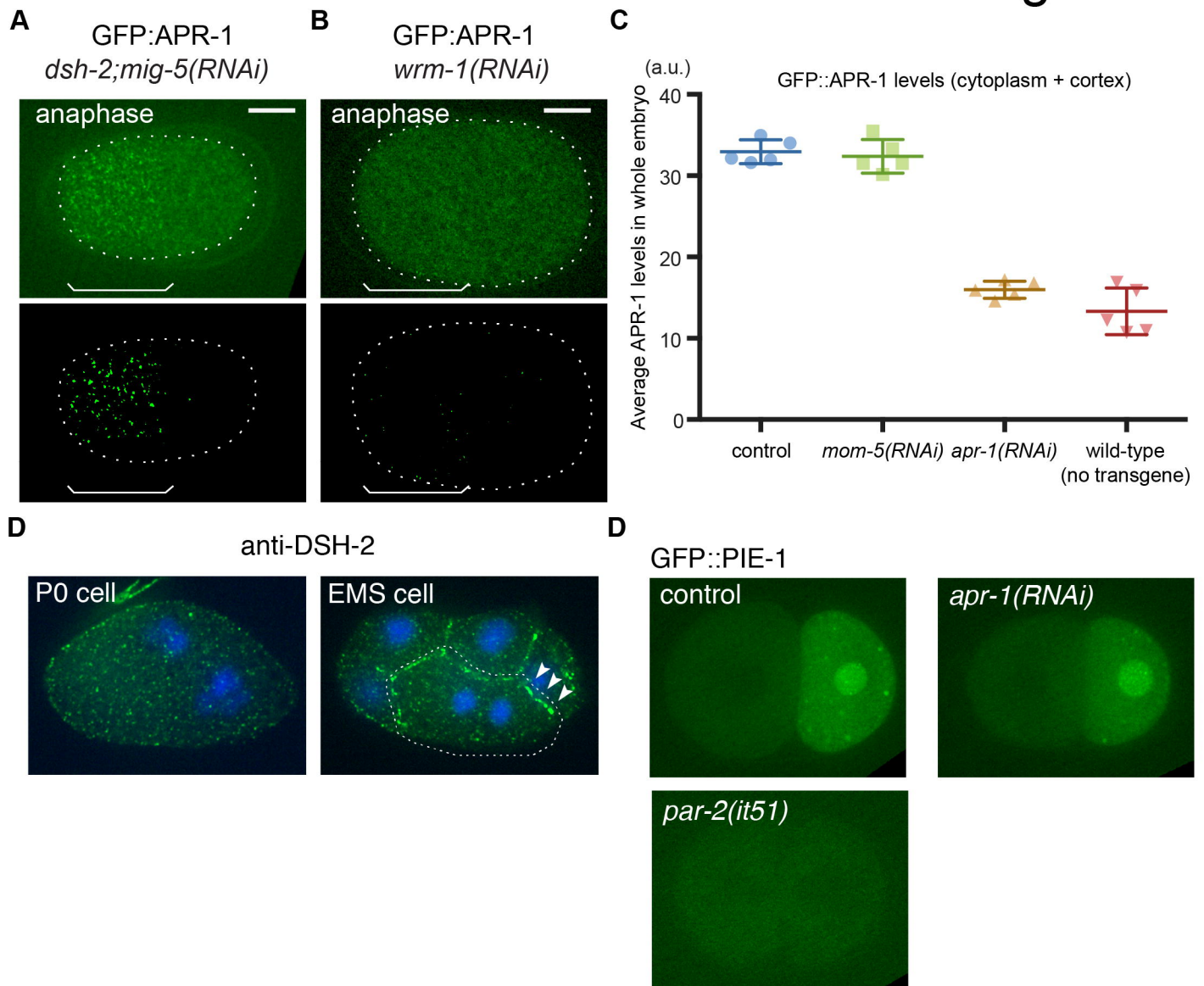


### Figure S2. Roles of Wnt signaling in APR-1 localization.

(A, B) Cell-surface GFP::APR-1 localization in RNAi of *dsh-2;mig-5*/dishevelled and *wrm-1*/ $\beta$ -catenin embryos. (C) Quantified GFP::APR-1 signal intensity per area of the whole embryo including the cell cortex and cytoplasm. (D) Immunofluorescence images of the DSH-2 protein during P0 and EMS cell division. Blue is DAPI staining. In EMS, the DSH-2 protein is enriched at the cell boundary between EMS and P2 (arrowheads) while no asymmetry was observed in P0. (E) Localizations of the cell fate determinant GFP::PIE-1 in the indicated genotypes. Control and *apr-1(RNAi)* shows PIE-1 enrichment in the posterior blastomere P1. In the *par-2* mutant, PIE-1 asymmetry was lost.

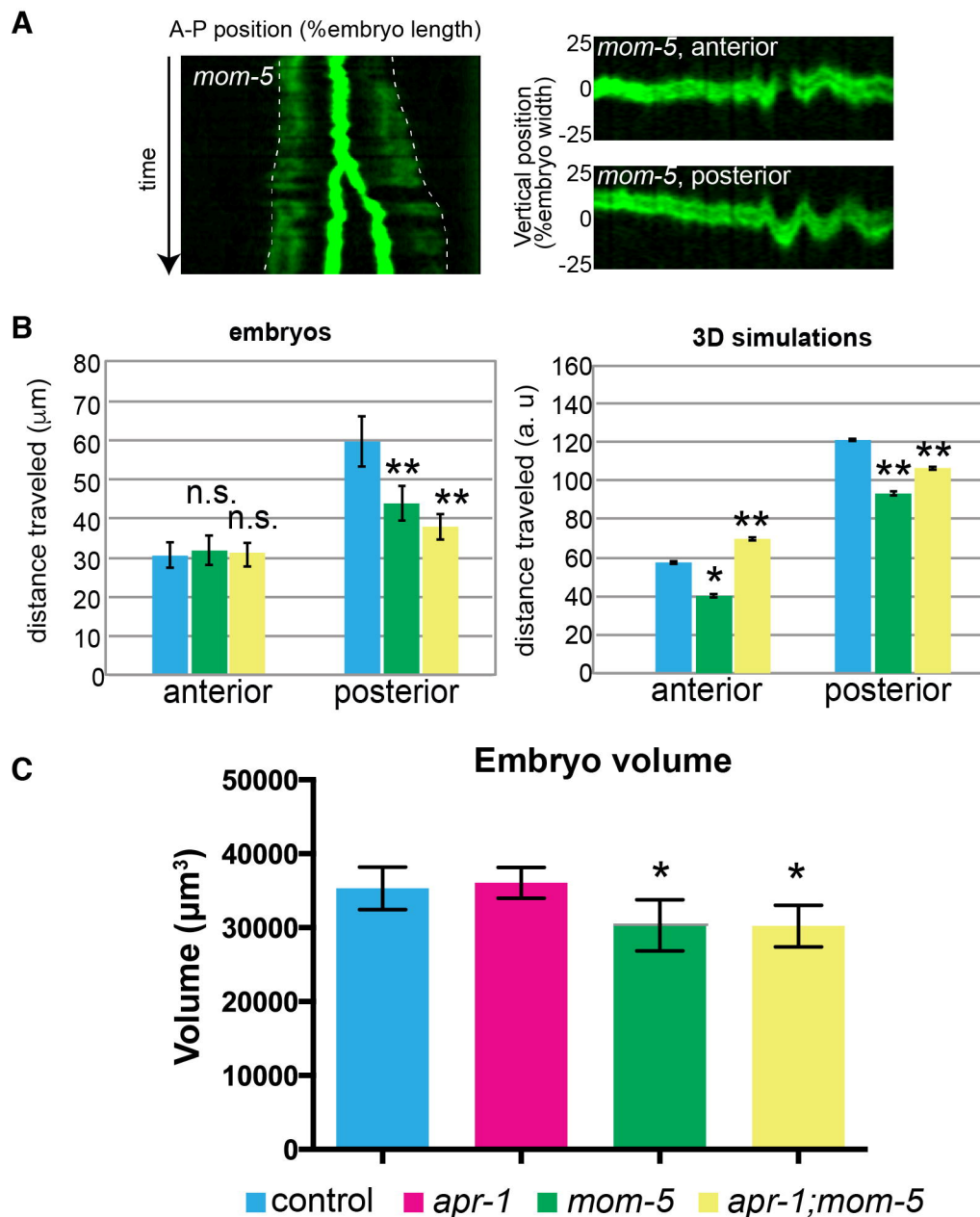


**Figure S3. Effects of *mom-5(RNAi)* on spindle pole movements and embryo sizes.**

(A) Kymographs of the spindle movements in *mom-5(RNAi)*. Kymographs were generated as in Figure 2. (B) Distance traveled by the anterior or posterior spindle poles. Total distance centrosome traveled for  $\pm 40$  sec and  $\pm 100$  sec of anaphase onset were shown for real embryos (left) and 3D simulations (right). (B) Cell volume of RNAi-treated embryos. Error bars show 95% CI. Asterisk indicate  $p < 0.05$  compared to control (Kruskal-Wallis test followed by Dunn's multiple comparison test).

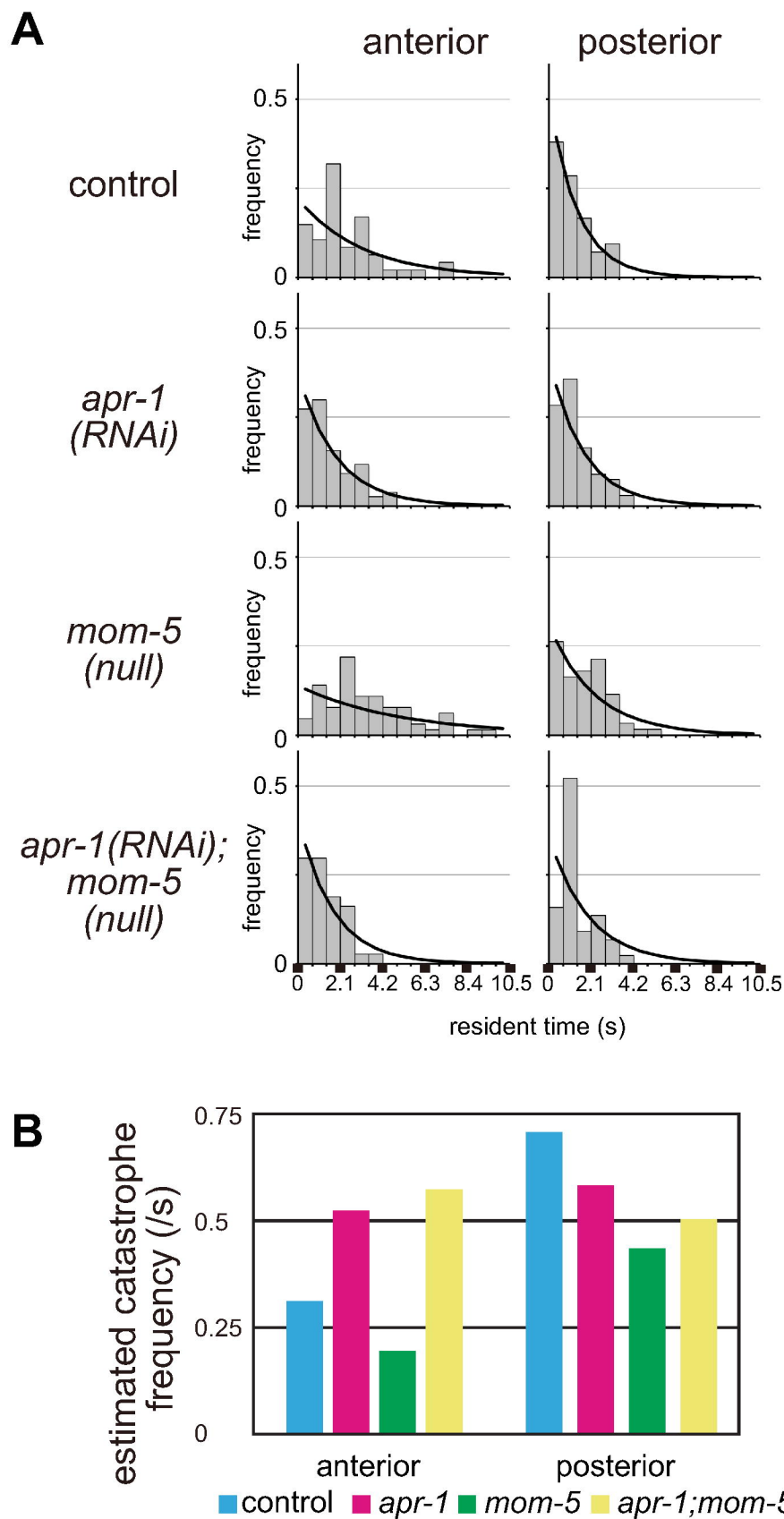


**Figure S4. Estimation of catastrophe frequencies at the cortex.**

(A) Frequencies of MT residence times at the cell cortex observed experimentally (histograms) and predicted from the estimated catastrophe frequencies (black lines). (B) Estimated catastrophe frequencies for indicated genotypes. The data is the same as in Supplementary Table 1.

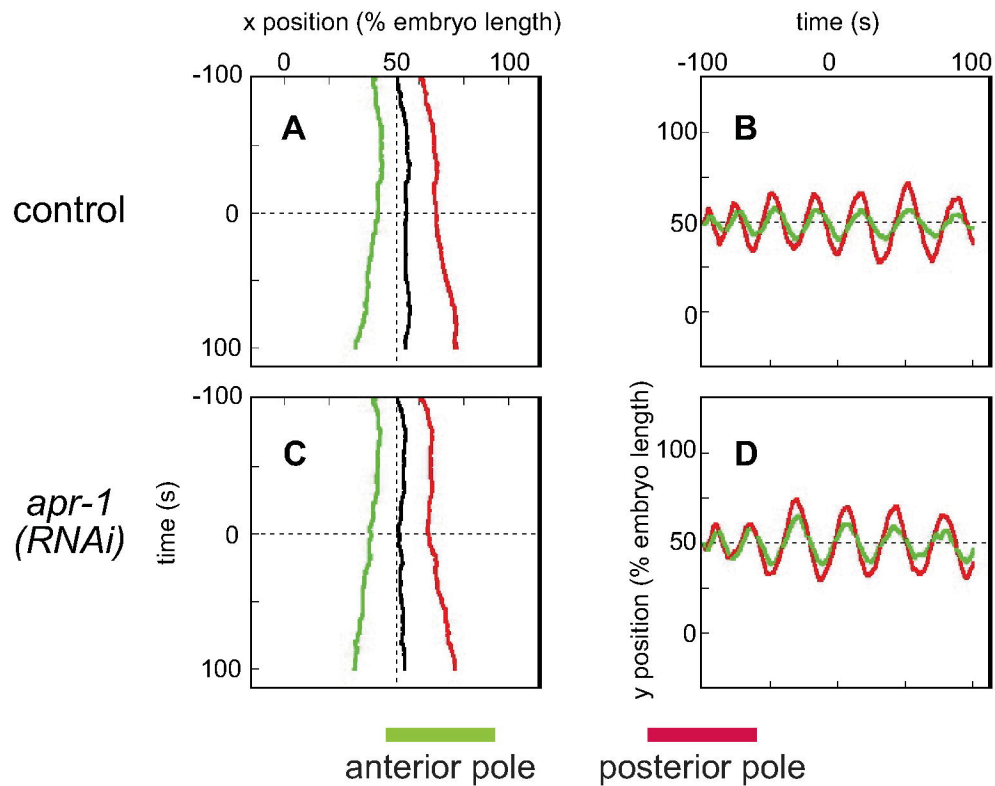


### Figure S5. Numerical simulation of spindle movements

(A-D) Representative trajectories of the spindle poles in the simulation. The trajectories of the anterior (green) and posterior (red) poles are shown. Their midpoint (black) is also shown in (A and D). (A, B) Control condition. (C, D) *apr-1(RNAi)* condition. (A and D) Trajectories along A-P axis (x axis). (C and E) and those along an axis perpendicular to the x axis (y axis) are shown.

**Table 1 Estimated catastrophe frequencies of the microtubules at the cortex**

	anterior cortex	posterior cortex
control (N2)	0.31 (/s)	0.72 (/s)
<i>apr-1</i>	0.53 (/s)	0.59 (/s)
<i>mom-5</i>	0.20 (/s)	0.44 (/s)
<i>apr-1; mom-5</i>	0.58 (/s)	0.51 (/s)

When catastrophe occurs stochastically with the frequency of  $\lambda$ , the probability distribution of the cortical residency time will be  $P(t) = \lambda \exp(-\lambda t)$ . Therefore, the probability of observing cortical residency time between  $t_1$  and  $t_2$  will be  $P(t_1 \sim t_2) = \exp(-\lambda t_1) - \exp(-\lambda t_2)$ . We fitted the experimentally obtained probability distribution of the cortical MT residency time to this equation to estimate the catastrophe frequencies of the MTs at the cortex

**Table 2. Parameter values used in the simulation**

		References
<b><i>Microtubule (MT) dynamics</i></b>		
Growth velocity ( $V_g$ ) [ $\mu\text{m/s}$ ]	0.328	(Srayko et al., 2005)
Shrinkage velocity ( $V_s$ ) [ $\mu\text{m/s}$ ]	0.537	(Kozłowski et al., 2007)
Catastrophe frequency ( $F_{\text{cat}}$ ) at cytoplasm [ $1/\text{s}$ ] <sup>a</sup>	0.046	(Kozłowski et al., 2007)
Rescue frequency ( $F_{\text{res}}$ ) [ $1/\text{s}$ ] <sup>b</sup>	1	
Number of fibers per pole	296	(Srayko et al., 2005)
<b><i>Pulling force, motor mediated</i></b>		
Stall force of motor ( $F_{\text{stall}}$ ) [pN]	1.1	(Gross et al., 2000)
Maximum velocity of motor ( $V_{\text{max}}$ ) [ $\mu\text{m/s}$ ]	2.0	(Gross et al., 2000)
<b><i>Pulling force, attachment of FG (cytoplasmic length dependent)</i></b>		
Density of motors ( $D$ ) [ $1/\mu\text{m}$ ]	0.2	
<b><i>Pulling force, attachment of FG (cortical)</i></b>		
Potential number of force generators at the cortex ( $N_{\text{potential, anterior}}$ , PAR-3 dependent)	15	
Potential number of force generators at the cortex ( $N_{\text{potential, posterior}}$ , PAR-2 dependent)	30	
The mean probability of the activation of the force generators ( $p_{\text{mean}}$ ) [ $1/\text{s}$ ]	0.5	(Pecreaux et al., 2006)
<b><i>Spindle as a spring</i></b>		
Natural length [ $\mu\text{m}$ ]	10-22	
Spring constant [pN/ $\mu\text{m}$ ]	1	
<b><i>Size of the cell</i></b>		
Long axis [ $\mu\text{m}$ ]	50	
Short axis [ $\mu\text{m}$ ]	30	
<b><i>Drag force of nucleus/spindle pole</i></b>		
Drag coefficient, for translational movement ( $\Gamma_{\text{trans}}$ ) [pN s/ $\mu\text{m}$ ] <sup>c</sup>	190	
Drag coefficient, for rotational movement ( $\Gamma_{\text{rot}}$ ) [pN s $\mu\text{m}$ ] <sup>c</sup>	25,000	
<b><i>Model-specific parameter</i></b>		
Time step [s]	0.01	

<sup>a</sup> See Table S1 for catastrophe frequency at the cortex

<sup>b</sup> A high frequency was used in this study. See text for a detailed explanation.

<sup>c</sup>  $6\pi\eta r$  for translational movement and  $8\pi^3\eta$  for rotational movement. Here, we set  $r$  (Stokes' radius) to 10  $\mu\text{m}$  and  $\eta$  (viscosity of the cytosol) to 1.0 pNs/ $\mu\text{m}^2$ .